

It’s a (Blind) Match!

Towards Vision-Language Correspondence without Parallel Data

Dominik Schnaus
TU Munich

Nikita Araslanov[†]
Munich Center for Machine Learning

Daniel Cremers[†]

Project page: [dominik-schnaus.github.io/itsamatch](https://github.com/dominik-schnaus/itsamatch)

[†] equal advising

Abstract

The platonic representation hypothesis suggests that vision and language embeddings become more homogeneous as model and dataset sizes increase. In particular, pairwise distances within each modality become more similar. This suggests that as foundation models mature, it may become possible to match vision and language embeddings in a fully unsupervised fashion, i.e. without parallel data. We present the first feasibility study, and investigate conformity of existing vision and language foundation models in the context of unsupervised, or “blind”, matching. First, we formulate unsupervised matching as a quadratic assignment problem and introduce a novel heuristic that outperforms previous solvers. We also develop a technique to find optimal matching problems, for which a non-trivial match is very likely. Second, we conduct an extensive study deploying a range of vision and language models on four datasets. Our analysis reveals that for many problem instances, vision and language representations can be indeed matched without supervision. This finding opens up the exciting possibility of embedding semantic knowledge into other modalities virtually annotation-free. As a proof of concept, we showcase an unsupervised classifier, which achieves non-trivial classification accuracy without any image-text annotation.

1. Introduction

Vision and language foundation models are changing the research landscape in computer vision and natural language processing. On the one hand, computer vision has widely adopted deep image representations, such as DINO [3], across virtually all applications, including semantic understanding [15] and 3D reconstruction [50]. On the other hand, large language models (LLMs) [e.g., 10] are already excelling at imitating natural language, performing comparably or better than humans in language translation and basic reasoning [e.g., see 53, for a survey]. Yet, we gravely lack in understanding the conformity between these mod-

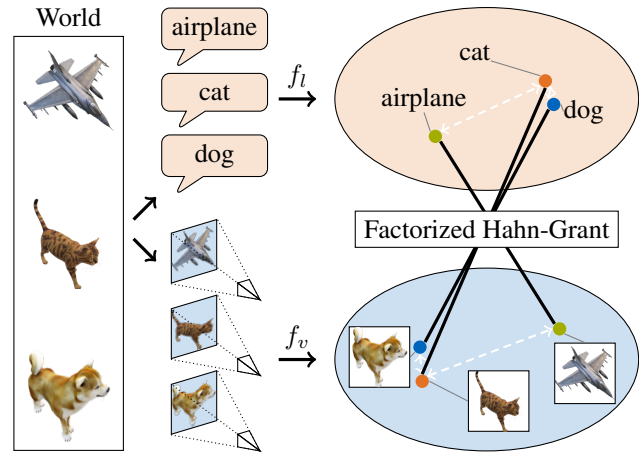


Figure 1. **Blind matching of vision and language:** Text and images are both abstractions of the same underlying world. Vision and language encoders f_v and f_l learn similar pairwise relations between concepts, e.g. “cat” is closer to “dog” than to “airplane”. We exploit these pairwise relations in our factorized Hahn-Grant solver to find valid correspondences between vision and language without any parallel data.

els. Previous work offers some analysis under the lens of a single modality or in the cross-modal scenario with focus on label efficiency [34, 35]. In particular, the latter body of work pursued dense alignment between vision and language embeddings from a few correspondences. Taking this scenario to the extreme, we study “blind” matching, illustrated in Fig. 1. Specifically, we aim to find vision-language correspondence without *any* parallel data.

Vision and language representations may seem incompatible at first. Indeed, there are significant differences in the training process, data distribution, and model architectures. However, the platonic representation hypothesis [17] posits that textual and visual representations of the same concepts converge to geometrically similar latent spaces. It asserts that models trained on large, diverse datasets encounter the same phenomena and, more importantly, the same relationships between the phenomena. As Fig. 1 con-

To appear in Proceedings of the *IEEE/CVF Conference on Computer Vision and Pattern Recognition (CVPR)*, Nashville, TN, USA, 2025.

ceptually illustrates, existing vision and language models already exhibit a high degree of vision-language compatibility. As Huh et al. [17] also show, the alignment grows with larger sizes of models and training corpora.

Capitalizing on the platonic representation hypothesis, we study vision-language alignment from a completely unsupervised perspective. Developing techniques towards such an analysis is valuable for two reasons. *First*, it will provide us with tools to study the conformity between vision and language models also on the abundance of unlabelled data. *Second*, establishing correspondence between semantic concepts (encapsulated by text) and images paves the way for purely unsupervised visual recognition. In fact, our study culminates in an intriguing proof-of-concept application, *unsupervised classifiers*, which perform (semantic) image recognition without any paired data.

Contributions. As our *technical* contribution to the study of blind vision-language alignment, we first formulate the task as a quadratic assignment problem (QAP). This formulation requires only pairwise distances within each modality as the input. We then discuss and analyze the metrics behind the pairwise relationships. Moving forward, we revisit and extend a solver for QAPs, exploiting a specialized heuristic towards memory-efficient and accurate vision-language matching. We thoroughly compare our solver extension with previous heuristics for QAPs and vision-language matching, establishing that our solver leads to better optima and provides tighter bounds. Lastly, we define optimal criteria for finding suitable subsets of matching problems as a p-dispersion-sum problem [24].

As our main *empirical* contribution, we conduct a large-scale study involving a total of 33 vision and 27 language models on four datasets. Our study reveals that despite the complexity of the underlying optimization problem, we can establish non-trivial solutions in some of the vision-language assignment problems across varying problem sizes. Intriguingly, this finding enables *unsupervised classification*: classifying images into semantic categories without any parallel supervision.

2. Related work

Vision and language foundation models. Unsupervised learning has enabled large-scale pre-training, both in the vision [3, 5, 16, 36] and language domains [7, 10, 43]. While semantics are inherent to language, the emergence of semantics in unsupervised vision models is yet not well-understood [3]. Unlike unimodal foundation models, joint vision-text encoders, such as CLIP [40] and ALBEF [26], as well as generative text-to-image models [41, 45], leverage a shared vision-language embedding space [42].

Zero-shot stitching. Zero-shot stitching recovers dense alignment between two embedding spaces, such as vision and text. Typically, the task assumes a sparse set of avail-

able ground-truth image-text pairs. Stitching two unimodal pre-trained vision and language encoders is possible using relative representations [34, 35], or with the help of a geometric distortion penalty [20]. Maiorca et al. [29] estimate an affine transform enabling vision-text alignment of pre-trained modality-specific encoders. Similar to our work, Maniparambil et al. [30] study the similarity of the embedding spaces in the vision and text-based encoders. However, their evaluation does not consider the fully unsupervised alignment, which is the main focus of our study.

Gromov-Wasserstein distance. One possibility to formulate the assignment problem between two sets is the Gromov-Wasserstein distance, which computes pairwise distances within each set. The exact computation of the Gromov-Wasserstein distance is NP-hard; thus, its practical application has remained limited. The few examples include shape matching [32], graph matching and partitioning [51, 52], and point-cloud matching [37]. Alvarez-Melis and Jaakkola [1] apply the Gromov-Wasserstein distance for cross-lingual alignment without parallel data. This approach realizes downstream tasks, such as word translation, in an unsupervised fashion. Chen et al. [4] leverage the Gromov-Wasserstein distance for cross-modal alignment in model training. In contrast to these works, we perform alignment between language and vision models without parallel data and any parameter training.

QAP solvers. The quadratic assignment problem (QAP) is generally NP-hard [46]. However, efficient approximations exist for specific problems [18, 38]. There are many heuristics for general QAPs, which can be divided into primal and dual methods [14]. The primal methods try to solve an approximation of the original problem, *e.g.* by relaxing the constraints or limiting the search space. These include the fast approximate QAP algorithm (FAQ) [49], the 2-opt algorithm [8], and optimal transport Gromov-Wasserstein methods [38]. Specific to our task, LocalCKA [30] uses the centered kernel alignment (CKA) metric and approximates the QAP with a linear assignment problem for finding vision-language correspondences. Dual methods maximize the dual of the QAP, *e.g.* by using block coordinate ascent [13] or subgradient methods [47]. For our heuristic, we use a dual ascent algorithm from operations research, which we refer to as Hahn-Grant solver [13] (and detail further in Sec. 4.1). Finally, many methods, including ours, combine primal and dual solvers. For example, Hutschenreiter et al. [18] uses fusion moves in combination with proposals from the dual formulation of the linearized QAP, thereby iteratively improving the objective. This has been shown as a useful heuristic for many computer vision problems [14]. Commercial solvers for QAPs exist, and we mainly compare with Gurobi [12], a highly optimized and general solver for mixed integer programming.

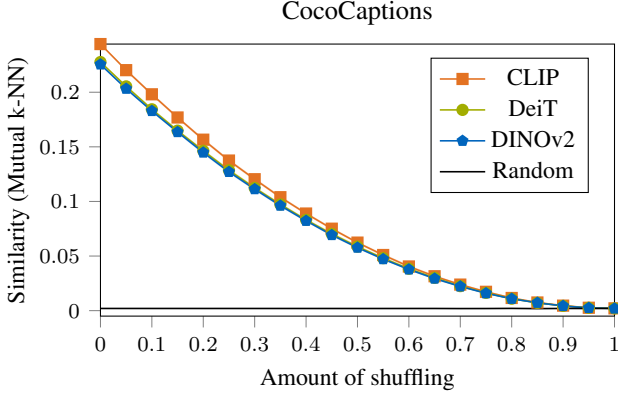


Figure 2. **Shuffling degrades vision-language alignment:** The vision-language alignment (here, measured by Mutual k-NN) monotonically decreases as we increasingly shuffle the oracle assignment. This holds for all considered metrics, justifying their use in the optimization objective. We encourage zooming in.

3. Preliminaries

Here, we establish the link between the vision and language embeddings by formulating an alignment problem via pairwise similarities within each modality.

Let us find a correspondence between vision and language representations of N classes. Given a set of images \mathcal{I}_i and text descriptions \mathcal{T}_i , we average their embeddings from a pre-trained vision model f_v and a language model f_l for each class $i \in \{1, \dots, N\}$:

$$\mathbf{x}_i = \frac{1}{|\mathcal{I}_i|} \sum_{I \in \mathcal{I}_i} f_v(I), \quad \mathbf{y}_i = \frac{1}{|\mathcal{T}_i|} \sum_{T \in \mathcal{T}_i} f_l(T). \quad (1)$$

Moreover, we L_2 -normalize each output of the model and the resulting averaged embeddings. We can then evaluate their similarity in each space individually using similarity measures k_x and k_y . The pairwise similarity matrices (or kernels) are then defined as

$$\mathbf{X}_{ij} = k_x(\mathbf{x}_i, \mathbf{x}_j) \text{ and } \mathbf{Y}_{ij} = k_y(\mathbf{y}_i, \mathbf{y}_j). \quad (2)$$

We measure the distortion of the pairwise similarities in vision and language spaces with a distance function $l(\cdot, \cdot)$. As its two arguments, the function takes the pairwise, possibly permuted, distance matrices from vision and language. Summing over all distortion elements yields the distortion between the vision and language embeddings:

$$\mathcal{D}_l(\mathbf{X}, \mathbf{Y}) = \sum_{i,j=1}^N l(\mathbf{X}_{ij}, \mathbf{Y}_{ij}). \quad (3)$$

Subject to a specific instantiation of $l(\cdot, \cdot)$, this formulation is general and can accommodate many existing distance (and similarity) measures. One notable example is

the Gromov-Wasserstein distance [33]. Other examples include the mutual k-nearest neighbors (Mutual k-NN) [17] and the centered kernel alignment (CKA) [22]. Note that these are similarity, not distance measures. Without loss of generality, we will use the negative inner product with these measures and build our theory around minimizing a distance measure (see Appx. B).

We now demonstrate that the pairwise distortion \mathcal{D}_l is indicative of vision-language alignment. Following Mani-parambil et al. [30], we begin with aligned matrices \mathbf{X} and \mathbf{Y} , and gradually permute the language similarity matrix \mathbf{Y} . For each permutation level, we randomly shuffle an increasing fraction of the language embeddings. We measure the alignment in terms of Mutual k-NN and define

$$\mathcal{D}_{\text{kNN}}(\mathbf{X}, \mathbf{Y}; \pi) = \sum_{i,j=1}^N l_{\text{kNN}}(\mathbf{X}_{ij}, \mathbf{Y}_{\pi(i)\pi(j)}), \quad (4)$$

where π is the random permutation. Mutual k-NN measures the average overlap between the nearest neighbors in both modalities. In Fig. 2, we report the results for the CocoCaptions dataset [6], where we sample 100 random permutations for each permutation level. We observe that \mathcal{D}_{kNN} decreases strictly monotonically as the amount of shuffling increases. This observation implies that, on average, pairwise distances between two semantically related vision and language embeddings are more similar than between two unrelated embeddings. We confirmed this behavior for all considered datasets (*e.g.*, ImageNet-100) and kernels (*e.g.*, Gromov-Wasserstein distance).¹

4. Blind matching of vision and language

We now show that the above formulation of the vision-language alignment in terms of minimizing \mathcal{D}_l leads to a quadratic assignment problem (QAP). Then, we introduce the factorized Hahn-Grant solver, which efficiently finds an approximate solution to the QAP.

QAP formulation. The previous experiment shows that well-aligned permutations tend to have high matching accuracy. Given unpaired vision and language data points, $\{\mathbf{x}_i\}$ and $\{\mathbf{y}_i\}$, we aim to find the permutation of rows and columns that minimizes their pairwise distortion, *i.e.*

$$\pi^* \in \arg \min_{\pi \in \Pi^N} \sum_{i,j=1}^N l(\mathbf{X}_{ij}, \mathbf{Y}_{\pi(i)\pi(j)}), \quad (5)$$

where Π^N is the permutation space, defined by bijective mappings from $\{1, \dots, N\}^N$ to $\{1, \dots, N\}^N$. This is a quadratic assignment problem (QAP), since by exchanging the permutation space with permutation matrices, we obtain

¹The results also hold for randomly initialized vision and language networks. See Appx. C for discussion and further results.

Algorithm 1 Hahn-Grant solver [13]

```

1: Input:  $\mathbf{C} \in \mathbb{R}_{\geq 0}^{N \times N \times N \times N}$  cost tensor
2: Output:  $l \leq \arg \min_{\mathbf{P} \in \mathcal{P}_N} \sum_{i,j,k,l=1}^N \mathbf{C}_{ijkl} \mathbf{P}_{ij} \mathbf{P}_{kl}$ 
3:  $l \leftarrow 0$ 
4: while not converged do
5:    $\text{leader}_{ij} \leftarrow \mathbf{C}_{ijij}$  for  $i, j \in [N]$ 
6:    $\mathbf{u}, \mathbf{v}, - \leftarrow \text{hungarian\_matching}(\text{leader})$ 
7:    $l \leftarrow l + \sum_i \mathbf{u}_i + \sum_j \mathbf{v}_j$ 
8:    $\text{leader}_{ij} \leftarrow \text{leader}_{ij} - \mathbf{u}_i - \mathbf{v}_j$  for  $i, j \in [N]$ 
9:    $\mathbf{C}_{ijkl} \leftarrow \mathbf{C}_{ijkl} + \frac{\text{leader}_{ij}}{N-1}$  for  $i \neq k, j \neq l \in [N]$ 
10:  for  $i, j \in [N]$  do
11:     $\mathbf{C}_{ijkl} \leftarrow \mathbf{C}_{ijkl} + \mathbf{C}_{klij}$  for  $i \neq k, j \neq l \in [N]$ 
12:     $\mathbf{C}_{klij} \leftarrow 0$  for  $i \neq k, j \neq l \in [N]$ 
13:     $\mathbf{u}, \mathbf{v}, - \leftarrow \text{hungarian\_matching}(\mathbf{C}_{i,j,[N] \setminus \{i\}, [N] \setminus \{j\}})$ 
14:     $\mathbf{C}_{ijij} \leftarrow \sum_k \mathbf{u}_k + \sum_l \mathbf{v}_l$ 
15:     $\mathbf{C}_{ijkl} \leftarrow \mathbf{C}_{ijkl} - \mathbf{u}_k - \mathbf{v}_l$  for  $i \neq k, j \neq l \in [N]$ 

```

Algorithm 2 Factorized Hahn-Grant solver (Ours)

```

1: Input:  $\mathbf{C}^{(1)}, \mathbf{C}^{(2)} \in \mathbb{R}_{\geq 0}^{N \times N}$  symmetric cost tensors
2: Output:  $l \leq \arg \min_{\mathbf{P} \in \mathcal{P}_N} \sum_{i,j,k,l=1}^N \mathbf{C}_{ik}^{(1)} \mathbf{C}_{jl}^{(2)} \mathbf{P}_{ij} \mathbf{P}_{kl}$ ,  $\mathbf{P}^* \in \mathcal{P}_N$  permutation matrix
3:  $l \leftarrow 0$ ;  $\mathbf{U}, \mathbf{V} \leftarrow \mathbf{0}_{N \times N \times N-1}$ ;  $\text{leader}_{ij} \leftarrow \mathbf{C}_{ii}^{(1)} \mathbf{C}_{jj}^{(2)}$ 
4:  $\mathbf{P}^* \leftarrow \text{primal\_heuristic}(\mathbf{C}^{(1)}, \mathbf{C}^{(2)})$ 
5: while not converged do
6:    $\mathbf{u}, \mathbf{v}, \mathbf{P} \leftarrow \text{lap\_solver}(\text{leader})$ 
7:    $\mathbf{P}^* \leftarrow \text{better}(\mathbf{P}^*, \mathbf{P})$ 
8:    $l \leftarrow l + \sum_i \mathbf{u}_i + \sum_j \mathbf{v}_j$ 
9:    $\text{leader}_{ij} \leftarrow \text{leader}_{ij} - \mathbf{u}_i - \mathbf{v}_j$  for  $i, j \in [N]$ 
10:   $\mathbf{U}_{ijk} \leftarrow \mathbf{U}_{ijk} - \frac{\text{leader}_{ij}}{N-1}$  for  $k \neq i, j \in [N]$ 
11:  for  $i, j \in [N]$  do
12:     $\mathbf{C}_{kl}^{\text{tmp}} \leftarrow 2\mathbf{C}_{ik}^{(1)} \mathbf{C}_{jl}^{(2)} - \mathbf{U}_{ijk} - \mathbf{V}_{ijl} - \mathbf{U}_{kli} - \mathbf{V}_{klj}$  for  $i \neq k, j \neq l \in [N]$ 
13:     $\mathbf{u}, \mathbf{v}, \mathbf{P} \leftarrow \text{lap\_solver}(\mathbf{C}^{\text{tmp}})$ 
14:     $\mathbf{P}^* \leftarrow \text{better}(\mathbf{P}^*, \mathbf{P})$ 
15:     $\text{leader}_{ij} \leftarrow \sum_k \mathbf{u}_k + \sum_l \mathbf{v}_l$ 
16:     $\mathbf{U}_{ijk} \leftarrow \mathbf{U}_{ijk} + \mathbf{u}_k$  for  $i \neq k \in [N]$ 
17:     $\mathbf{V}_{ijl} \leftarrow \mathbf{V}_{ijl} + \mathbf{v}_l$  for  $j \neq l \in [N]$ 

```

Figure 3. **The Hahn-Grant solver (left) and the factorized Hahn-Grant solver (ours, right):** The Hahn-Grant solver [13] iteratively improves the dual bound of the QAP by solving linear assignment problems (LAPs). Our solver has higher memory efficiency for factorized cost matrices. We also use a faster solver for the LAPs and a primal heuristic that recycles the assignment from the LAPs.

$$\mathbf{P}^* \in \arg \min_{\mathbf{P} \in \mathcal{P}_N} \sum_{i,j,k,l=1}^N l(\mathbf{X}_{ik}, \mathbf{Y}_{jl}) \mathbf{P}_{ij} \mathbf{P}_{kl}. \quad (6)$$

Here, \mathcal{P}_N is the group of permutation matrices, *i.e.* binary matrices in which the columns and the rows sum up to one:

$$\mathcal{P}_N = \{\mathbf{P} \mid \mathbf{P} \in \{0, 1\}^{N \times N}, \mathbf{P}\mathbf{1} = \mathbf{1}, \mathbf{P}^T \mathbf{1} = \mathbf{1}\}. \quad (7)$$

4.1. The factorized Hahn-Grant solver

Solving the QAP in Eq. (6) by enumeration is not scalable, because there are $N!$ different permutations. Furthermore, finding the global optimum for a general QAP is NP-hard [46]. In practice, even proprietary solvers like Gurobi [12] already fail for problem instances of size $N < 30$ (see Sec. 5.3). Nevertheless, as we discussed in Sec. 2, one can recover the global solution or approximate it to a sufficient degree for some specific problem domains [38, 49]. Our main technical contribution is an extension of the Hahn-Grant solver that allows efficient matching of vision and language without any paired data.

The Hahn-Grant solver. The Hahn-Grant solver (*cf.* Algorithm 1) produces tight lower bounds for QAPs [13]. It iteratively transforms a QAP with a non-negative cost ten-

sor \mathbf{C} into an equivalent form:

$$\sum_{i,j,k,l=1}^N \mathbf{C}_{ijkl} \mathbf{P}_{ij} \mathbf{P}_{kl} = l + \sum_{i,j=1}^N \text{leader}_{ij} \mathbf{P}_{ij} + \sum_{i,j,k,l=1}^N (\mathbf{C}_{ijkl} - \mathbf{u}_k^{(ij)} - \mathbf{v}_l^{(ij)}) \mathbf{P}_{ij} \mathbf{P}_{kl}. \quad (8)$$

The solver transfers the cost from the quadratic term to a linear and then a constant term by solving linear assignment problems (LAPs). The cost of the LAPs from the quadratic term can then be moved to `leader` (Lines 13-14), and the cost from the `leader` LAP can be moved to the constant term (Lines 6-7). On the other hand, the dual solutions of the LAPs are subtracted from the cost tensor and `leader` (Line 8 and Line 15). Moreover, in each step, both \mathbf{C}_{ijkl} and \mathbf{C}_{klij} are used to improve the dual (Lines 11-12). At the end of each step, the non-zero values of `leader` are evenly distributed back to the corresponding submatrices in \mathbf{C} (Line 9). Because of the redistribution, the next iteration can use these values to make further progress. The algorithm terminates once no improvement can be made. This means that the `leader` LAP can be solved with cost zero. Therefore, each of the LAPs corresponding to non-zero indices of the solution also has a zero-cost solution. If there is a permutation matrix that solves all of these LAPs, one has found the global optimum. In the algorithm, the constant

l maintains a lower bound of the original QAP. Since we solve $N^2 + 1$ LAPs in each iteration, the algorithm has a total runtime of $\mathcal{O}(N^5)$ and a memory complexity of $\mathcal{O}(N^4)$.

The factorized Hahn-Grant solver. We adapt the Hahn-Grant solver for vision-language matching with three key extensions: (1) We also search for primal solutions, (2) reduce the memory complexity from $\mathcal{O}(N^4)$ to $\mathcal{O}(N^3)$, and (3) use a faster solver for the LAPs.

We search for primal solutions in two stages. First, we initialize the problem with the FAQ [49] and 2opt [8] heuristics, using the best result from 100 random seeds (Line 4). Second, we evaluate the solutions of each LAP on the QAP (Line 7 and Line 14). This does not add considerable overhead, because the assignment was already calculated as a by-product. Therefore, we only need to evaluate the QAP objective functions once more. If the algorithm converges to a solution, that solution also needs to solve at least one of the LAPs [13], and our heuristic will find the global optimum. If the algorithm does not converge, we output the lowest-cost solution found during the run.

To reduce the memory requirements, we first observe that the commonly used distortion measures $l(\cdot, \cdot)$ are decomposable as

$$l(A, B) = f_1(A) + f_2(B) - h_1(A)h_2(B). \quad (9)$$

This includes the squared L_2 -distance, Kullback-Leibler divergence [38], and the negative Frobenius inner product, which we use for the centered kernel alignment (CKA) and the Mutual k-NN. Given such a decomposable measure, the original QAP is equivalent to

$$\mathbf{P}^* \in \arg \min_{\mathbf{P} \in \mathcal{P}_N} \sum_{i,j,k,l=1}^N \mathbf{C}_{ik}^{(1)} \mathbf{C}_{jl}^{(2)} \mathbf{P}_{ij} \mathbf{P}_{kl}. \quad (10)$$

This is an instance of a Koopmans-Beckmann QAP [21] with cost matrices $\mathbf{C}^{(1)} = -h_1(\mathbf{X})$ and $\mathbf{C}^{(2)} = h_2(\mathbf{Y})$. Although these are only two $N \times N$ matrices, applying the Hahn-Grant solver would require us to compute and store the full tensor \mathbf{C} . Instead of updating this tensor in-place, we store them separately in \mathbf{U} and \mathbf{V} . Therefore, the memory requirement is only $\mathcal{O}(N^3)$, instead of $\mathcal{O}(N^4)$.

Finally, we also experimented with the auction and the Jonker-Volgenant algorithm, instead of the Hungarian algorithm [25]. Despite the expected runtime of $\mathcal{O}(N^4 \log N)$ for the auction algorithm [2], we observed a faster convergence in all of our experiments using a specialized C++ implementation [31] of the Jonker-Volgenant algorithm [19] with a total asymptotic runtime of $\mathcal{O}(N^5)$. Appx. D provides more details and a thorough comparison between our solver and the original Hahn-Grant solver.

4.2. Finding optimal matching problems

Despite the strong correlation between the distortion metric and the matching accuracy (cf. Fig. 2), the accuracy varies

significantly depending on the choice of categories. This implies that a non-trivial matching for an arbitrary choice of semantic categories is not guaranteed. Nevertheless, we can find a subset of matching problems where a non-trivial match is very likely, even for large problem sizes ($N > 10$).

Using the enumeration approach to find an optimal category subset is already infeasible for small problem sizes. For example, finding a matching problem of size $N = 10$ in a dataset with 100 categories involves a search space of size $\binom{100}{10}$. However, we can explicitly formulate the problem of finding an optimal subset as an optimization problem. For a subset of classes $S \subset \{1, \dots, L\}$, the alignment is given by

$$A(S) = \sum_{i,j \in S} l(\mathbf{X}_{ij}, \mathbf{Y}_{ij}). \quad (11)$$

Therefore, we can find the subset S that maximizes the alignment, *i.e.*

$$S^* \in \arg \max_S A(S), \quad (12)$$

where the variable S satisfies $S \subset \{1, \dots, L\}$ and $|S| = N$. Formulating this problem as a quadratic binary optimization problem [24], we obtain

$$\mathbf{s}^* \in \arg \max_{\mathbf{s}} \sum_{i,j=1}^N l(\mathbf{X}_{ij}, \mathbf{Y}_{ij}) \mathbf{s}_i \mathbf{s}_j, \quad (13)$$

$$\text{s.t. } \mathbf{s} \in \{0, 1\}^L \text{ and } \mathbf{s}^T \mathbf{1} = N. \quad (14)$$

The non-zero entries of \mathbf{s}^* correspond to the classes in the subset S^* . This problem is an instance of the p-dispersion-sum problem [24]. Although the problem is NP-hard in general [39], we can find reasonable approximations using Gurobi, as we demonstrate in Sec. 5.2.

5. Experiments

Our experiments encompass three studies and an example application. Our first study in Sec. 5.1 focuses on a small problem size ($N = 10$), where we can analyze the properties of the global solution in a tractable manner. We find that for an overwhelming number of pre-trained vision and language models, the optimal solutions w.r.t. the Gromov-Wasserstein distance correspond to non-trivial matching between the two modalities, well above the random chance. Sec. 5.2 presents the second study, where we employ our factorized Hahn-Grant solver to find solutions of larger-scale problems. This study reveals that there is a subset of larger matching problems where our solver finds a non-trivial match *without any paired data*. The third study in Sec. 5.3 compares our factorized Hahn-Grant solver to alternative optimization algorithms in terms of solution optimality. In particular, we observe that only the global optimum corresponds to non-trivial results. Finally, Sec. 5.4

extends these studies with an exciting application, introducing unsupervised classifiers.

Pre-trained models. In total, we consider 33 vision models and 27 language models using a variety of pre-trainings, architectures and sizes. For vision, we use self-supervised (DINO [3], DINOv2 [36]), fully-supervised (DeiT [48], ConvNeXt [27]), and vision-language supervised (CLIP [42]) models. For language, we use different models from the SentenceTransformers library [43] and CLIP [42]. Appx. E elaborates further.

Setup. Given an image classification dataset, we extract the vision embeddings for each image and compute the average vision embedding for each class. Similarly, we average the language embedding from multiple prompts to get a language representation. To observe the effect of small perturbations in the pairwise distances on the matching, we compute the vision representation using random subsets of the data. In our preliminary analysis, we found the Gromov-Wasserstein distance to be superior to CKA for matching vision and language.² Therefore, we use the Gromov-Wasserstein distance in all upcoming experiments.

5.1. Small-scale matching

Setup. For small matching problems (*e.g.* $N = 10$), we can exactly enumerate the solution space, which offers an ideal testbed for our Gromov-Wasserstein measure. We perform matching on CIFAR-10 [23] and CINIC-10³ [9].

Results. We show the matching accuracy for different vision models in Fig. 4. On the left, we use all-mpnet-base-v2 evaluated on CIFAR-10 and, on the right, All-Roberta-large-v1 on CINIC-10. More combinations are given in Appx. F.1. We observe that *most models perform better than 10% accuracy*, which is the baseline for random permutations. Moreover, the DINOv2 model can be matched with the highest accuracy of 72% on CIFAR-10 and 100% on CINIC-10. Curiously, we observe that it is the pre-training strategy that seems to have a larger impact than the model size. On average for all language models, the DINOv2 models are 5.2% better on CIFAR-10 and 7.7% better on CINIC-10 than the second-best pre-training strategy.

5.2. Larger-scale matching

We now investigate matching of larger problems ($N > 10$). For vision-language matching, a larger problem implies a finer granularity of the classes (apart from the computational considerations). This means that the pairwise distances must consistently encode more nuanced similarities.

Setup. We evaluate the matching accuracy on subsets of different sizes for ImageNet-100 [44] and CIFAR-100 [23]. Following Sec. 4.2, we hypothesize that not all classes are

²See Appx. B for the comparison.

³CINIC-10 is a subset of ImageNet [44] with 10 classes from CIFAR-10. Our only adaption is that we keep the image resolution from ImageNet.

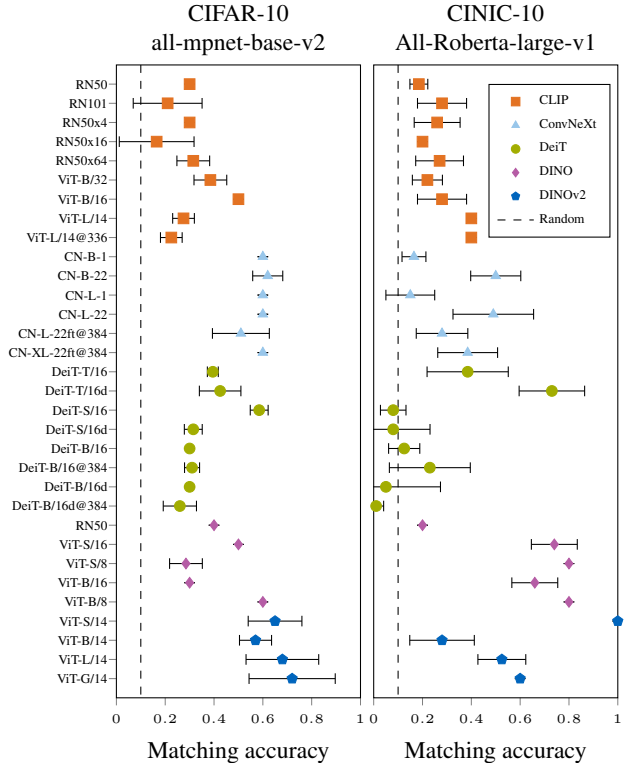


Figure 4. **Most vision and language models can be matched non-trivially:** We visualize the accuracy for multiple vision models with the all-mpnet-base-v2 [43] language model on CIFAR-10 [23] (left) and with the All-Roberta-large-v1 [43] language model on CINIC-10 [9] (right). The error bar shows the standard deviation for 20 random seeds and the dashed line shows the performance of random matching. Observe that most vision representations can be matched with high accuracy to language, and the pre-training method has a greater impact than the model size. DINOv2 [36] achieves the highest accuracy, on average.

represented similarly. Therefore, we use our optimization problem from Sec. 4.2 to find subsets of classes that are well-aligned. We evaluate the alignment of the largest DINOv2, CLIP, and DeiT models with all-mpnet-base-v2.

Results Fig. 5 summarizes the results for this experiment for ImageNet-100 (Fig. 5, left) and for CIFAR-100 (Fig. 5, right). We observe that *all models have high accuracy for small problem sizes*, and that performance drops for larger problem sizes. Thus, for each model, there is a set of classes that is represented similarly. However, some categories adversely affect the matching, suggesting their different representation in vision and language models. As somewhat expected, CLIP outperforms the other two models in most cases, indicating that more classes share similar representation with the language model for CLIP than for DeiT and DINOv2. On CIFAR-100, the performance of DINOv2 declines more sharply than for the other models. Thus, some classes degrade the matching, if added. These

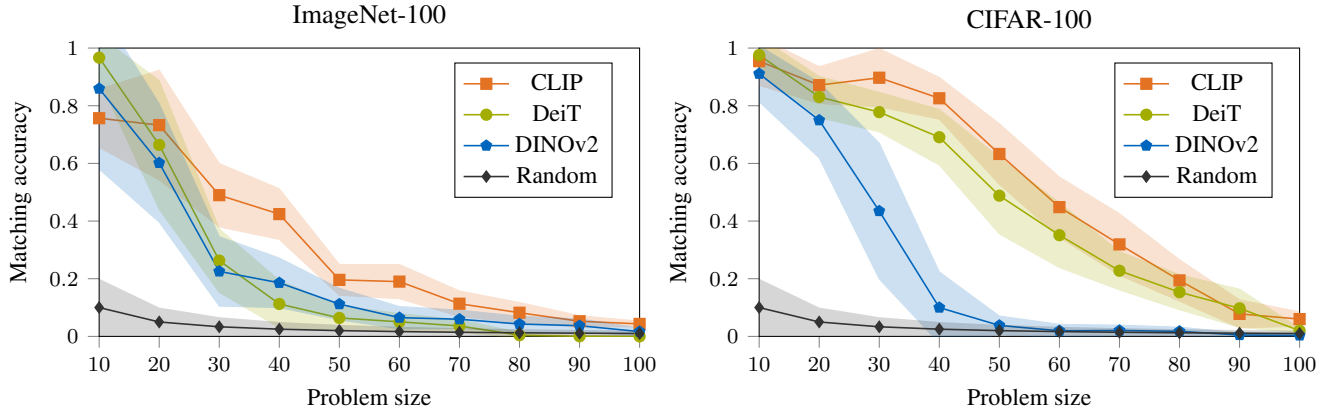


Figure 5. **Some fine-grained problems can be matched with high accuracy:** For each problem size, we select the optimal ten subsets of classes using the optimization from Sec. 4.2 on ImageNet-100 [44] (left) and CIFAR-100 [23] (right). We show the matching accuracy for all optimization problems, each with three random seeds for the vision models DINOv2 [36], CLIP [42], and DeiT [48] using the all-mpnet-base-v2 language model [43]. We observe that we can find optimization problems, especially for $N < 40$, that lead to accurate matching. On both datasets, CLIP performs best for most problem sizes.

results suggest that language supervision during training can align pairwise similarities, especially for fine-grained classes. Nevertheless, the self-supervised DINOv2 also learns aligned pairwise distances for some of the classes.

5.3. Solver comparison

We now show that previous solvers are often unable to obtain meaningful assignments for our matching problems.

Setup. We compare the solvers both in the small-scale setting from Sec. 5.1 and in the larger-scale setting using the optimal matching problems. We compare to the computer vision solver MPOpt [18], the commercial solver Gurobi [12], the fast approximate QAP algorithm (FAQ) [49], entropic Gromov-Wasserstein optimal transport (OT)⁴ [38], and LocalCKA [30]. For both experiments, we use CLIP ViT-L/14@336px and all-mpnet-base-v2. More details and other settings are available in Appx. F.3.

Results. In the small-scale setting, we can compute the global optimum with enumeration. In Tab. 1, we compare the matching accuracy, the cost after optimization, and the percentage that the global optimum is reached for every method. For LocalCKA, the CKA metric is minimized using a linear approximation. We observe that minimizing this approximation does not lead to better results than random permutations, both in terms of Gromov-Wasserstein loss and the matching accuracy. Both local solvers (OT, FAQ) are able to minimize the loss, but are stuck in a local minimum, thus their accuracy is not better than the random baseline. This shows that *local optima are not sufficient to find a useful match*. MPOpt manages to approach the optimal objective, but only reaches it about half the time. In contrast, both our heuristic and Gurobi find the global opti-

Solver	Accuracy (%)	Cost	Global? (%)
Random	10±10	1.73±0.30	0±0
LocalCKA [30]	10±9	1.77±0.27	0±0
OT [38]	2±4	0.64±0.11	0±0
FAQ [49]	1±3	0.62±0.08	0±0
MPOpt [18]	49±12	0.36±0.02	50±51
Gurobi [12]	60±0	0.34±0.02	100±0
Ours	60±0	0.34±0.02	100±0

Table 1. **Solver comparison on small-scale problems:** Using CLIP [42] and all-mpnet-base-v2 [43] on CINIC-10 [9], we report the matching accuracy, the Gromov-Wasserstein distance (cost), and the frequency of the global optimum. Most of the previous solvers fail to find the global optimum. We also observe that local optima are not sufficient to achieve a meaningful matching accuracy. By contrast, our solver always finds the global optimum, leading to the highest matching accuracy.

um every time, resulting in accuracy of 60%.

Fig. 6 reports the results on the larger-scale problem. We show the cost and the lower bound for each problem size. For ease of comparison and for computational reasons, we select only one set of classes for each problem size. Consistent with the small-scale experiment, LocalCKA does not perform better than random and produces out-of-bound values. Interestingly, OT and FAQ are able to solve some instances with global optimality. We suspect that this is because the optimal problem may have a specialized structure. Therefore, the relaxations can lead to the global optimum for such problems. Already at size 30, all but our method fail to reach the global optimum. For problem sizes larger than 60, Gurobi does not produce a solution within the given time limit. *Our method consistently provides the tightest*

⁴See Appx. G for how to use OT for QAPs.

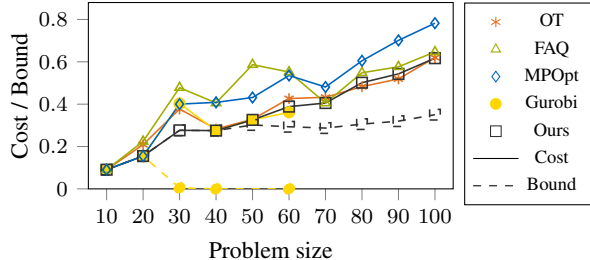


Figure 6. **Solver comparison on larger-scale problems:** Using CLIP and all-mpnet-base-v2 on CIFAR-100 [23], we plot the Gromov-Wasserstein distance (solid line) and its lower bound (dashed line) where available. Costs from LocalCKA [30] and MPOpt bounds are outside axis limits. For problems over 60, Gurobi exceeds the 1.5-hour time limit. Across all sizes, our solver yields tighter bounds and better primal solutions most of the time, achieving global optimality up to size 40.

Model	All-Roberta-large-v1 (%)	all-mpnet-base-v2 (%)
CLIP	29.2±0.5	28.5±0.4
DeiT	46.7±3.4	21.8±7.5
DINOv2	51.5±9.2	38.8±0.4

Table 2. **Unsupervised classification:** We combine our unsupervised matching with K-Means clustering of the image embeddings on CIFAR-10 [23]. It shows that using the cluster means as vision representation is enough to get a non-trivial accuracy. This is a good example of how unsupervised matching can enable a completely new application without supervision.

bounds, provably leading to a global optimum up to size 40. Furthermore, it achieves the best primal solution for most sizes, even surpassing Gurobi on problems of size 30.

5.4. Application: Unsupervised classifiers

We introduce a proof-of-concept application exploiting our formulation of the unsupervised vision-language matching.

Setup. Assuming no annotation, we cluster image representations using K-Means [28]. We use the cluster centers for one-to-one matching with language embeddings using our QAP formulation, relying only on the pairwise distances. Given the solution, the elements of each cluster acquire the label of the corresponding language embedding.

Results. We evaluate our unsupervised classifier with several vision and language models in Tab. 2. The best accuracy is achieved by the DINOv2 model with 51.5% for All-Roberta-large-v1. However, all of the considered models achieve a higher accuracy than the random baseline of 10%. These results are clearly inferior to the supervised models. Nevertheless, to the best of our knowledge, *this is the first instance of fully unsupervised classification.* Furthermore, we show in Appx. F.2 that previous solvers are not able to find meaningful matches in this setting and analyze how clustering changes the matching performance.

6. Discussion

Can we match vision and language without paired data?

Our small-scale experiments (*cf.* Sec. 5.1) indeed suggest that most vision and language models can be matched with high accuracy. This implies that on the tested datasets, the pairwise relations are similar. Furthermore, our larger-scale experiment (*cf.* Sec. 5.2) shows that it is also possible to match larger sets of fine-grained concepts. However, it also shows that some classes have different representation in vision and language, hence cannot be matched reliably.

Can we match arbitrary embeddings?

Not with existing models yet. Our larger-scale experiments in Sec. 5.2 show that vision and language models may encode semantic concepts differently. This is not surprising, since some concepts are abstract and appear only in one of the modalities, *e.g.* “freedom of speech” [17]. For such concepts, conforming vision-language embedding spaces without explicit supervision are highly unlikely. Another issue is symmetry: vision-language matching may be ambiguous due to multiple (equivalent) local minima. Finally, the computational complexity scales in the order of $\mathcal{O}(N^5)$. Therefore, our solver does not scale to problems of sizes larger than those studied in Sec. 5.2. Even for problems of size 100, the bound between the primal and the dual is significant. Thus, reaching the global optimum becomes infeasible.

Which vision model can be matched best?

Our small-scale experiment in Sec. 5.1 indicates that DINOv2 models can be matched best. However, on CIFAR-100 in the large-scale experiment, we observe that CLIP and DeiT perform better, especially on larger problems. This suggests that DINOv2 consistently represents broader concepts, whereas CLIP and DeiT better encode fine-grained relationships.

7. Conclusion

In this work, we investigated the “blind” alignment of vision and language embedding spaces, *i.e.* without parallel data. Our contribution combines a technical and an empirical element. As a technical contribution, we showed that unsupervised alignment is an instance of a quadratic assignment problem, QAP. This problem formulation includes only the pairwise similarities in each embedding space. We proposed a new heuristic for solving the QAP, outperforming previous solvers on the alignment problem. On the empirical side, we extensively study the alignment of pre-trained vision and language models. Our analysis establishes feasibility of a non-trivial match between vision and language. Although solving general and large-scale matching problems remains an open challenge, the established feasibility creates exciting avenues for novel applications. The presented proof-of-concept unsupervised classifier is an intriguing first step in this direction.

Acknowledgments. We thank the anonymous reviewers for their valuable feedback. This work was supported by the Federal Ministry for the Environment, Nature Conservation, Nuclear Safety and Consumer Protection (BMUV) through the AuSeSol-AI project (grant 67KI21007A), and by the TUM Georg Nemetschek Institute Artificial Intelligence for the Built World (GNI) through the AICC project.

References

- [1] David Alvarez-Melis and Tommi S. Jaakkola. Gromov-Wasserstein alignment of word embedding spaces. In *EMNLP*, pages 1881–1890, 2018. 2
- [2] Dimitri P. Bertsekas. A distributed algorithm for the assignment problem. *Lab. Inf. Decis. Syst. Working Paper, MIT*, 1979. 5
- [3] Mathilde Caron, Hugo Touvron, Ishan Misra, Hervé Jégou, Julien Mairal, Piotr Bojanowski, and Armand Joulin. Emerging properties in self-supervised vision transformers. In *ICCV*, pages 9630–9640, 2021. 1, 2, 6, vi
- [4] Liqun Chen, Zhe Gan, Yu Cheng, Linjie Li, Lawrence Carin, and Jingjing Liu. Graph optimal transport for cross-domain alignment. In *ICML*, pages 1542–1553, 2020. 2
- [5] Ting Chen, Simon Kornblith, Mohammad Norouzi, and Geoffrey E. Hinton. A simple framework for contrastive learning of visual representations. In *ICML*, pages 1597–1607, 2020. 2
- [6] Xinlei Chen, Hao Fang, Tsung-Yi Lin, Ramakrishna Vedantam, Saurabh Gupta, Piotr Dollár, and C Lawrence Zitnick. Microsoft COCO captions: Data collection and evaluation server. *arXiv:1504.00325 [cs.CV]*, 2015. 3, ii
- [7] Aakanksha Chowdhery, Sharan Narang, Jacob Devlin, and Maarten Bosma et al. PaLM: Scaling language modeling with pathways. *J. Mach. Learn. Res.*, 24:240:1–240:113, 2023. 2
- [8] Georges A. Croes. A method for solving traveling-salesman problems. *Operations research*, 6(6):791–812, 1958. 2, 5
- [9] Luke N. Darlow, Elliot J. Crowley, Antreas Antoniou, and Amos J. Storkey. CINIC-10 is not ImageNet or CIFAR-10. *arXiv:1810.03505 [cs.CV]*, 2018. 6, 7, ii, vi
- [10] Jacob Devlin, Ming-Wei Chang, Kenton Lee, and Kristina Toutanova. BERT: Pre-training of deep bidirectional transformers for language understanding. In *NAACL-HLT*, pages 4171–4186, 2019. 1, 2
- [11] Alexey Dosovitskiy, Lucas Beyer, Alexander Kolesnikov, Dirk Weissenborn, Xiaohua Zhai, Thomas Unterthiner, Mostafa Dehghani, Matthias Minderer, Georg Heigold, Sylvain Gelly, Jakob Székely, and Neil Houlsby. An image is worth 16x16 words: Transformers for image recognition at scale. In *ICLR*, 2021. ii
- [12] Gurobi Optimization, LLC. Gurobi Optimizer Reference Manual, 2024. 2, 4, 7, vii, viii, xii
- [13] Peter Hahn and Thomas Grant. Lower bounds for the quadratic assignment problem based upon a dual formulation. *Operations Research*, 46(6):912–922, 1998. 2, 4, 5, iii, v
- [14] Stefan Haller, Lorenz Feineis, Lisa Hutschenreiter, Florian Bernard, Carsten Rother, Dagmar Kainmüller, Paul Swoboda, and Bogdan Savchynskyy. A comparative study of graph matching algorithms in computer vision. In *ECCV*, pages 636–653, 2022. 2
- [15] Mark Hamilton, Zhoutong Zhang, Bharath Hariharan, Noah Snavely, and William T. Freeman. Unsupervised semantic segmentation by distilling feature correspondences. In *ICLR*, 2022. 1
- [16] Kaiming He, Xinlei Chen, Saining Xie, Yanghao Li, Piotr Dollár, and Ross B. Girshick. Masked autoencoders are scalable vision learners. In *CVPR*, pages 15979–15988, 2022. 2
- [17] Minyoung Huh, Brian Cheung, Tongzhou Wang, and Phillip Isola. Position: The platonic representation hypothesis. In *ICML*, pages 20617–20642, 2024. 1, 2, 3, 8, i, ii, viii
- [18] Lisa Hutschenreiter, Stefan Haller, Lorenz Feineis, Carsten Rother, Dagmar Kainmüller, and Bogdan Savchynskyy. Fusion moves for graph matching. In *ICCV*, pages 6270–6279, 2021. 2, 7, viii, xii
- [19] Roy Jonker and Ton Volgenant. A shortest augmenting path algorithm for dense and sparse linear assignment problems. *Computing*, 38(4):325–340, 1987. 5, v
- [20] Dustin Klebe, Tal Shnitzer, Mikhail Yurochkin, Leonid Karlinsky, and Justin Solomon. GeRA: Label-efficient geometrically regularized alignment. *arXiv:2310.00672 [cs.LG]*, 2023. 2
- [21] Tjalling C. Koopmans and Martin Beckmann. Assignment problems and the location of economic activities. *Econometrica*, pages 53–76, 1957. 5
- [22] Simon Kornblith, Mohammad Norouzi, Honglak Lee, and Geoffrey Hinton. Similarity of neural network representations revisited. In *ICML*, pages 3519–3529, 2019. 3, i, ii
- [23] Alex Krizhevsky. Learning multiple layers of features from tiny images. Technical report, 2009. 6, 7, 8, ii, vi
- [24] Michael J. Kuby. Programming models for facility dispersion: The p-dispersion and maximum dispersion problems. *Geogr. Analysis*, 19(4):315–329, 1987. 2, 5
- [25] Harold W. Kuhn. The hungarian method for the assignment problem. *Nav. Res. Logist. Q.*, 2(1-2):83–97, 1955. 5
- [26] Junnan Li, Ramprasaath R. Selvaraju, Akhilesh Gotmare, Shafiq R. Joty, Caiming Xiong, and Steven Chu-Hong Hoi. Align before fuse: Vision and language representation learning with momentum distillation. In *NeurIPS*, pages 9694–9705, 2021. 2
- [27] Zhuang Liu, Hanzi Mao, Chao-Yuan Wu, Christoph Feichtenhofer, Trevor Darrell, and Saining Xie. A convnet for the 2020s. In *CVPR*, pages 11976–11986, 2022. 6, vi
- [28] Stuart Lloyd. Least squares quantization in pcm. *Trans. Inf. Theory*, 28(2):129–137, 1982. 8, viii
- [29] Valentino Maiorca, Luca Moschella, Antonio Norelli, Marco Fumero, Francesco Locatello, and Emanuele Rodolà. Latent space translation via semantic alignment. In *NeurIPS*, 2023. 2
- [30] Mayug Maniparambil, Raiymbek Akshulakov, Yasser Abdelaziz Dahou Djilali, Sanath Narayan, Mohamed El Amine Seddik, Kartikeya Mangalam, and Noel E. O’Connor. Do vision and language encoders represent the world similarly? *arXiv:2401.05224 [cs.CV]*, 2024. 2, 3, 7, 8, i, xi, xii
- [31] Vadim Markovtsev. Linear assignment problem solver using Jonker-Volgenant algorithm. <https://github.com/src-d/lapjv>, 2017. 5, v

- [32] Facundo Mémoli. Gromov-wasserstein distances and the metric approach to object matching. *Found. Comput. Math.*, 11(4):417–487, 2011. [2](#)
- [33] Facundo Mémoli. Gromov-wasserstein distances and the metric approach to object matching. *Foundations of computational mathematics*, 11:417–487, 2011. [3](#), [i](#), [ii](#)
- [34] Luca Moschella, Valentino Maiorca, Marco Fumero, Antonio Norelli, Francesco Locatello, and Emanuele Rodolà. Relative representations enable zero-shot latent space communication. In *ICLR*, 2023. [1](#), [2](#)
- [35] Antonio Norelli, Marco Fumero, Valentino Maiorca, Luca Moschella, Emanuele Rodolà, and Francesco Locatello. ASIF: Coupled data turns unimodal models to multimodal without training. In *NeurIPS*, 2023. [1](#), [2](#), [vii](#)
- [36] Maxime Oquab, Timothée Darcet, and Théo Moutakanni et al. DINOv2: Learning robust visual features without supervision. *TMLR*, 2024. [2](#), [6](#), [7](#), [ii](#), [vi](#)
- [37] Gabriel Peyré, Marco Cuturi, and Justin Solomon. Gromov-Wasserstein averaging of kernel and distance matrices. In *ICML*, pages 2664–2672, 2016. [2](#)
- [38] Gabriel Peyré, Marco Cuturi, and Justin Solomon. Gromov-Wasserstein averaging of kernel and distance matrices. In *ICML*, pages 2664–2672, 2016. [2](#), [4](#), [5](#), [7](#), [ii](#), [xi](#), [xii](#)
- [39] David Pisinger. *Exact solution of p-dispersion problems*. DIKU, 1999. [5](#)
- [40] Alec Radford, Jong Wook Kim, Chris Hallacy, Aditya Ramesh, Gabriel Goh, Sandhini Agarwal, Girish Sastry, Amanda Askell, Pamela Mishkin, Jack Clark, Gretchen Krueger, and Ilya Sutskever. Learning transferable visual models from natural language supervision. In *ICML*, pages 8748–8763, 2021. [2](#)
- [41] Aditya Ramesh, Mikhail Pavlov, Gabriel Goh, Scott Gray, Chelsea Voss, Alec Radford, Mark Chen, and Ilya Sutskever. Zero-shot text-to-image generation. In *ICML*, 2021. [2](#)
- [42] Aditya Ramesh, Prafulla Dhariwal, Alex Nichol, Casey Chu, and Mark Chen. Hierarchical text-conditional image generation with CLIP latents. *arXiv:2204.06125 [cs.CV]*, 2022. [2](#), [6](#), [7](#), [vi](#)
- [43] Nils Reimers and Iryna Gurevych. Sentence-BERT: Sentence embeddings using siamese bert-networks. In *EMNLP-IJCNLP*, pages 3980–3990, 2019. [2](#), [6](#), [7](#), [ii](#), [vi](#)
- [44] Olga Russakovsky, Jia Deng, Hao Su, Jonathan Krause, Sanjeev Satheesh, Sean Ma, Zhiheng Huang, Andrej Karpathy, Aditya Khosla, Michael S. Bernstein, Alexander C. Berg, and Li Fei-Fei. ImageNet large scale visual recognition challenge. *Int. J. Comput. Vis.*, 115(3):211–252, 2015. [6](#), [7](#), [vi](#)
- [45] Chitwan Saharia, William Chan, and Saurabh Saxena et al. Photorealistic text-to-image diffusion models with deep language understanding. In *NeurIPS*, 2022. [2](#)
- [46] Sartaj Sahni and Teofilo Gonzalez. P-complete approximation problems. *JACM*, 23(3):555–565, 1976. [2](#), [4](#)
- [47] Lorenzo Torresani, Vladimir Kolmogorov, and Carsten Rother. A dual decomposition approach to feature correspondence. *IEEE TPAMI*, 35(2):259–271, 2012. [2](#)
- [48] Hugo Touvron, Matthieu Cord, Matthijs Douze, Francisco Massa, Alexandre Sablayrolles, and Hervé Jégou. Training data-efficient image transformers & distillation through attention. In *ICML*, pages 10347–10357, 2021. [6](#), [7](#), [vi](#)
- [49] Joshua T. Vogelstein, John M. Conroy, Vince Lyzinski, Louis J. Podrazik, Steven G. Kratzer, Eric T. Harley, Donnell E. Fishkind, R. Jacob Vogelstein, and Carey E. Priebe. Fast approximate quadratic programming for graph matching. *PLOS One*, 10(4), 2015. [2](#), [4](#), [5](#), [7](#), [xi](#), [xii](#)
- [50] Shangzhe Wu, Ruining Li, Tomas Jakab, Christian Rupprecht, and Andrea Vedaldi. MagicPony: Learning articulated 3d animals in the wild. In *CVPR*, pages 8792–8802, 2023. [1](#)
- [51] Hongteng Xu, Dixin Luo, and Lawrence Carin. Scalable Gromov-Wasserstein learning for graph partitioning and matching. In *NeurIPS*, pages 3046–3056, 2019. [2](#)
- [52] Hongteng Xu, Dixin Luo, Hongyuan Zha, and Lawrence Carin. Gromov-wasserstein learning for graph matching and node embedding. In *ICML*, pages 6932–6941, 2019. [2](#)
- [53] Wayne Xin Zhao, Kun Zhou, and Junyi Li et al. A survey of large language models. *arXiv:2303.18223 [cs.CL]*, 2023. [1](#)

It’s a (Blind) Match!

Towards Vision-Language Correspondence without Parallel Data

Supplementary Material

A. Overview

- Appx. B shows that our QAP formulation is general enough to accommodate the commonly used distance and similarity measures: Mutual k-NN, CKA and the Gromov-Wasserstein distance.
- Appx. C follows up on the experiment in Sec. 3. It shows that the vision-language similarity measured by our distortion metrics decreases as the amount of shuffling increases. Furthermore, it elaborates on why randomly initialized networks exhibit a similar trend to pre-trained networks.
- Appx. D compares the original Hahn-Grant solver to our factorized Hahn-Grant solver including a correctness proof, implementation details and an ablation showing the improvements in primal and dual estimates by our solver.
- Appx. E gives more details on the used models, datasets and specific setups for the individual experiments.
- Appx. F provides results for other model and dataset combinations. It shows that pre-training appears more important than the model size for the matching accuracy in small-scale alignment. Also, it shows that the results for solver comparison consistently hold for all considered model and dataset combinations including unsupervised classification.
- Appx. G shows that the Gromov-Wasserstein optimal transport solvers can be seen as solvers for a relaxation of our QAP.

B. Mutual k-NN and CKA as distortion metrics

In Sec. 4, we introduce the notation of distortion metrics in terms of a unimodal kernel function k_x and k_y , and a distance function l , which is decomposable as

$$l(A, B) = f_1(A) + f_2(B) - h_1(A)h_2(B). \quad (15)$$

In this section, we show how Mutual k-NN [17], the centered kernel alignment (CKA) [22], and the Gromov-Wasserstein (\mathcal{GW}) distance [33] fit into this formulation.

Mutual k-NN [17]. Mutual k-NN is defined as the average overlap between the nearest neighbors in both modalities, *i.e.*, for one sample, it is

$$m_{\text{kNN}}(\mathbf{x}_i, \mathbf{y}_i) = \frac{1}{k} |\text{top}_k^{\mathbf{x}}(i) \cap \text{top}_k^{\mathbf{y}}(i)|. \quad (16)$$

Here, we define the top- k indices in terms of the highest inner product as $\text{top}_k^{\mathbf{x}}(i)$. Following Huh et al. [17], we exclude i from this set. To include this into our framework,

we define the kernel function as

$$k_x^{\text{kNN}}(\mathbf{x}_i, \mathbf{x}_j) = \frac{1}{\sqrt{Nk}} \mathbb{1}[j \in \text{top}_k^{\mathbf{x}}(i)], \quad (17)$$

and accordingly for the language embeddings. Then, the similarity matrices are

$$\mathbf{X}_{ij}^{\text{kNN}} = k_x^{\text{kNN}}(\mathbf{x}_i, \mathbf{x}_j) \text{ and } \mathbf{Y}_{ij}^{\text{kNN}} = k_y^{\text{kNN}}(\mathbf{y}_i, \mathbf{y}_j). \quad (18)$$

Furthermore, we use the negative inner product as our distortion function:

$$l_{\text{inner}}(A, B) = -A \cdot B, \quad (19)$$

which trivially satisfies Eq. (15) with $f_1 = f_2 = 0$ and h_1, h_2 being identity functions. This choice of kernels and the distance metric leads to the Mutual k-NN metric in our framework:

$$\begin{aligned} \mathcal{D}_{\text{kNN}}(\mathbf{X}^{\text{kNN}}, \mathbf{Y}^{\text{kNN}}) &= \sum_{i,j=1}^N l(\mathbf{X}_{ij}^{\text{kNN}}, \mathbf{Y}_{ij}^{\text{kNN}}) \\ &= - \sum_{i,j=1}^N k_x^{\text{kNN}}(\mathbf{x}_i, \mathbf{x}_j) k_y^{\text{kNN}}(\mathbf{y}_i, \mathbf{y}_j) \\ &= - \sum_{i,j=1}^N \frac{1}{\sqrt{Nk}} \mathbb{1}[j \in \text{top}_k^{\mathbf{x}}(i)] \frac{1}{\sqrt{Nk}} \mathbb{1}[j \in \text{top}_k^{\mathbf{y}}(i)] \\ &= - \frac{1}{N} \sum_{i,j=1}^N \frac{1}{k} \mathbb{1}[j \in \text{top}_k^{\mathbf{x}}(i) \wedge j \in \text{top}_k^{\mathbf{y}}(i)] \\ &= - \frac{1}{N} \sum_{i,j=1}^N \frac{1}{k} \mathbb{1}[j \in \text{top}_k^{\mathbf{x}}(i) \cap \text{top}_k^{\mathbf{y}}(i)] \\ &= - \frac{1}{N} \sum_{i=1}^N \frac{1}{k} |j \in \text{top}_k^{\mathbf{x}}(i) \cap \text{top}_k^{\mathbf{y}}(i)| \\ &= - \frac{1}{N} \sum_{i=1}^N m_{\text{kNN}}(\mathbf{x}_i, \mathbf{y}_i). \end{aligned} \quad (20)$$

CKA. We derive CKA [22, 30] in a similar fashion. For a kernel function \hat{k} and kernel matrices $\hat{\mathbf{X}}_{ij} = \hat{k}(\mathbf{x}_i, \mathbf{x}_j)$ and $\hat{\mathbf{Y}}_{ij} = \hat{k}(\mathbf{y}_i, \mathbf{y}_j)$, the CKA is defined as

$$\text{CKA}(\hat{\mathbf{X}}, \hat{\mathbf{Y}}) = \frac{\text{tr}(\hat{\mathbf{X}}\hat{\mathbf{C}}\hat{\mathbf{Y}}\hat{\mathbf{C}})}{\sqrt{\text{tr}(\hat{\mathbf{X}}\hat{\mathbf{C}}\hat{\mathbf{X}}\hat{\mathbf{C}}) \text{tr}(\hat{\mathbf{Y}}\hat{\mathbf{C}}\hat{\mathbf{Y}}\hat{\mathbf{C}})}}, \quad (21)$$

where $\hat{\mathbf{C}} = \mathbf{I} - \frac{1}{N} \mathbb{1} \mathbb{1}^T$. Similar to previous work [30], we

Models	CIFAR-10 (%)	CINIC-10 (%)
Mutual k-NN	30.5 ± 16.7	16.5 ± 27.6
CKA	42.0 ± 4.1	40.0 ± 0.0
\mathcal{GW} distance	72.0 ± 17.7	77.0 ± 7.3

Table 3. **Gromov-Wasserstein distance is the best measure for matching:** We show the accuracy for CIFAR-10 [23] and CINIC-10 [9] using DINOv2 [36] and all-mpnet-base-v2 [43] using Mutual k-nearest neighbor (Mutual k-NN) [17], centered kernel alignment (CKA) [22], and the Gromov-Wasserstein (\mathcal{GW}) distance [33] as a metric. The \mathcal{GW} distance leads to the best matching accuracy for both datasets.

use the linear kernel in this work. Our kernel matrices are

$$\begin{aligned} \mathbf{X}^{\text{CKA}} &= \frac{\hat{\mathbf{X}}\mathbf{C}}{\sqrt{\text{tr}(\hat{\mathbf{X}}\mathbf{C}\hat{\mathbf{X}}\mathbf{C})}} \quad \text{and} \\ \mathbf{Y}^{\text{CKA}} &= \frac{\mathbf{C}^T\hat{\mathbf{Y}}^T}{\sqrt{\text{tr}(\hat{\mathbf{Y}}\mathbf{C}\hat{\mathbf{Y}}\mathbf{C})}}. \end{aligned} \quad (22)$$

Using the negative inner product as the distance metric leads to the negative CKA:

$$\begin{aligned} D_{\text{CKA}}(\mathbf{X}^{\text{CKA}}, \mathbf{Y}^{\text{CKA}}) & \\ &= \sum_{i,j=1}^N l(\mathbf{X}_{ij}^{\text{CKA}}, \mathbf{Y}_{ij}^{\text{CKA}}) \\ &= - \sum_{i,j=1}^N \frac{(\hat{\mathbf{X}}\mathbf{C})_{ij} (\mathbf{C}^T\hat{\mathbf{Y}}^T)_{ij}}{\sqrt{\text{tr}(\hat{\mathbf{X}}\mathbf{C}\hat{\mathbf{X}}\mathbf{C})} \sqrt{\text{tr}(\hat{\mathbf{Y}}\mathbf{C}\hat{\mathbf{Y}}\mathbf{C})}} \\ &= - \frac{1}{\sqrt{\text{tr}(\hat{\mathbf{X}}\mathbf{C}\hat{\mathbf{X}}\mathbf{C})} \sqrt{\text{tr}(\hat{\mathbf{Y}}\mathbf{C}\hat{\mathbf{Y}}\mathbf{C})}} \sum_{i,j=1}^N (\hat{\mathbf{X}}\mathbf{C})_{ij} (\hat{\mathbf{Y}}\mathbf{C})_{ji} \\ &= - \frac{1}{\sqrt{\text{tr}(\hat{\mathbf{X}}\mathbf{C}\hat{\mathbf{X}}\mathbf{C})} \sqrt{\text{tr}(\hat{\mathbf{Y}}\mathbf{C}\hat{\mathbf{Y}}\mathbf{C})}} \text{tr}(\hat{\mathbf{X}}\mathbf{C}\hat{\mathbf{Y}}\mathbf{C}) \\ &= -\text{CKA}(\hat{\mathbf{X}}, \hat{\mathbf{Y}}) \end{aligned} \quad (23)$$

\mathcal{GW} distance [33]. For the \mathcal{GW} distance, we can choose the L_2 -norm as the kernel and the squared distance as the distortion metric:

$$\begin{aligned} k_x^{\mathcal{GW}}(\mathbf{x}_i, \mathbf{x}_j) &= \|\mathbf{x}_i - \mathbf{x}_j\|_2, \\ k_y^{\mathcal{GW}}(\mathbf{y}_i, \mathbf{y}_j) &= \|\mathbf{y}_i - \mathbf{y}_j\|_2, \\ l_{\mathcal{GW}}(A, B) &= (A - B)^2. \end{aligned} \quad (24)$$

Then, the \mathcal{GW} distance is given by

$$D_{\mathcal{GW}}(\mathbf{X}^{\mathcal{GW}}, \mathbf{Y}^{\mathcal{GW}}) = \sum_{i,j=1}^N (\|\mathbf{x}_i - \mathbf{x}_j\|_2 - \|\mathbf{y}_i - \mathbf{y}_j\|_2)^2. \quad (25)$$

The objective function after finding the optimal permutation matrix similar to Eq. (6) is then equivalent to the original \mathcal{GW} distance comparing two metric-measure spaces [38].

Tab. 3 empirically compares these formulations in a small-scale data regime, using CIFAR-10 [23] and CINIC-10 [9] datasets introduced in the main text. We find that despite the wider adoption of Mutual k-NN and CKA metrics in previous work, the Gromov-Wasserstein distance leads to a higher matching accuracy on both datasets.

C. Shuffled vision-language alignment

In this section, we elaborate on the setup for the shuffling experiment from Sec. 3. As we claimed in the main text (*cf.* Sec. 3), the observations are consistent across all tested datasets and models, which we also report here.

Setup. Given aligned image and language representations, $(\mathbf{x}_i, \mathbf{y}_i)$, and a shuffling level $\alpha \in [0, 1]$, we randomly choose $\lfloor \alpha N \rfloor$ elements that are randomly permuted. Every other element is kept in place. Afterwards, the distortion of this permutation is computed with Eq. (3) or Eq. (4) after the permutation. Note that we use the image embeddings here instead of the averaged object embeddings. For classification datasets, we take the same language embedding for all elements of that class. However, we have seen in preliminary experiments that the curve looks similar when considering the averaged object representations instead of the image representations. We plot 21 equidistant shuffling levels at $\alpha \in \{0, 0.05, \dots, 1\}$. Each level is based on 100 random seeds to sample the subset and permutation.

Shuffling with other kernels, datasets, and models. In addition to Fig. 2, which uses the CocoCaptions dataset [6], and Mutual k-NN as the distortion metric, we show more combinations in Fig. 7. In this setting, Mutual k-NN is only meaningful for paired datasets because the k-nearest neighbors are ambiguous when language features are replicated. For the \mathcal{GW} distance, the pairwise distances are also dependent on the dimensionality of the embedding spaces. Therefore, we standardize the distance to be in the range between zero and one for this shuffling experiment. We observe that the similarity (l distortion) decreases (l increases) strongly monotonically with more shuffling. This behavior is consistent for all considered datasets and metrics. This observation suggests that the pairwise relations are more similar between the semantically corresponding vision and language representations than between the non-semantic ones.

A note on randomly initialized networks. In Fig. 8, we present a plot of the experiment in Fig. 2 with the addition of randomly initialized ViT-H/14 [11] models, which were initiated with 20 distinct random seeds. Additionally, we demonstrate the distortion of a representation based on the stacked pixel values, *i.e.*, without any neural network. Furthermore, we show a zoomed-in version on the left-hand side to illustrate the behavior on a finer scale.

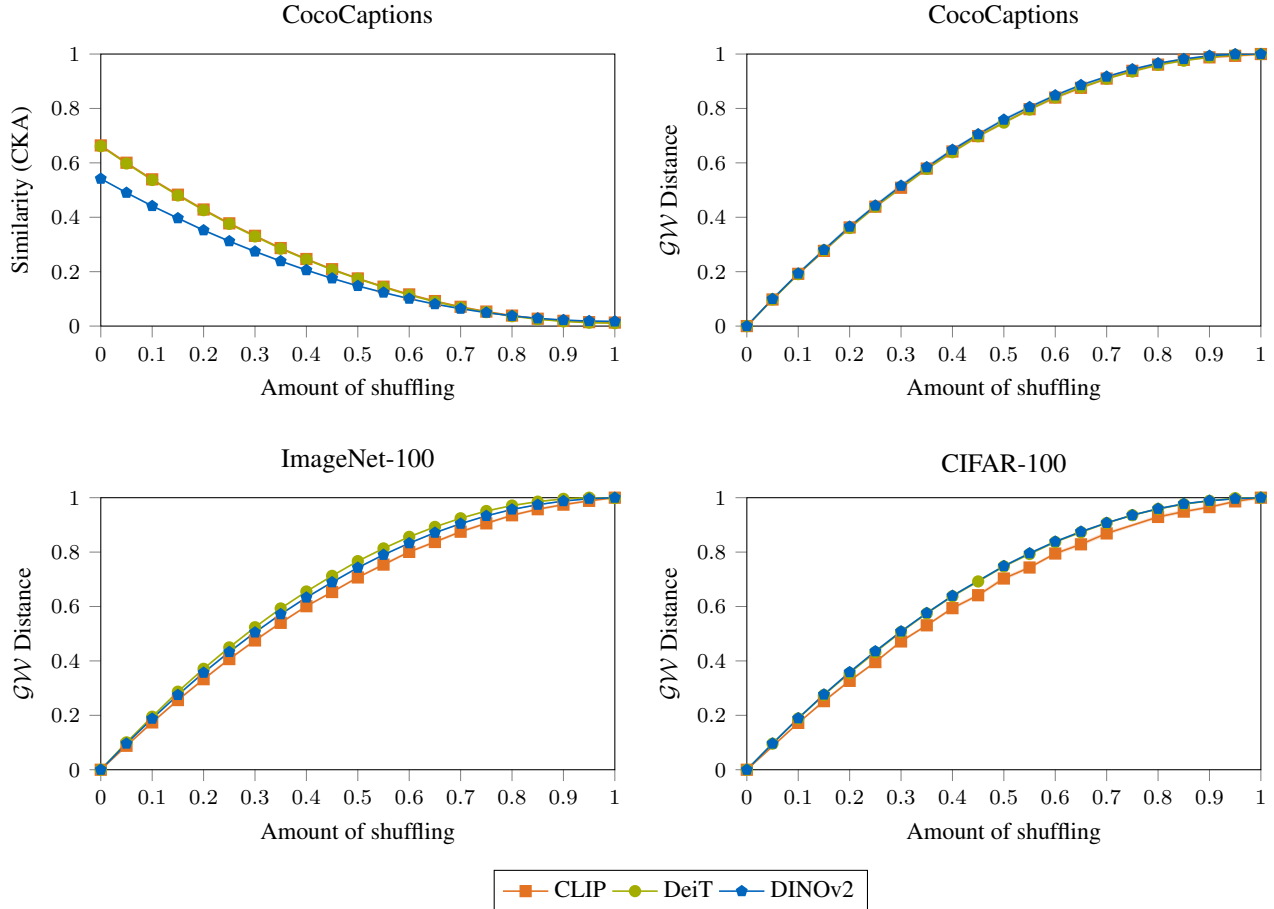


Figure 7. **Shuffling degrades vision-language alignment:** We report CKA similarity and the Gromov-Wasserstein distance on three datasets and based on five encoding methods, including pre-trained and randomly initialized networks, and raw pixel values. Similar to our observation with Mutual k-NN, the CKA and Gromov-Wasserstein distance correlate strongly w.r.t. the amount of shuffling, which suggests that these metrics are also suitable measures for blind vision-language matching.

We observe that the alignment of randomly initialized networks exhibits the same monotonically decreasing behavior with increased amount of shuffling, as for pre-trained networks (despite the absolute alignment value being smaller). For images, this can be explained by the similarity of the pixel distribution within each semantic category (e.g., a green landscape for animal stock). These similarities appear more frequently for semantically affiliated classes and can dominate the pairwise distance encoding. To understand the behavior for randomly initialized networks, we plot the distribution of the *Empirical Lipschitz constant* in Fig. 9, defined by

$$\mathcal{K}_{\text{Lipschitz}}(\mathbf{x}, \mathbf{y}) = \frac{\|f(\mathbf{x}) - f(\mathbf{y})\|_2}{\|\mathbf{x} - \mathbf{y}\|_2}, \quad (26)$$

for samples \mathbf{x} , \mathbf{y} and function f . Intuitively, it measures the degree of distance distortion in the output space w.r.t. the input space for each sample pair in the dataset. Here, we use CocoCaptions and the same language model as in Fig. 8.

We observe that most values are close to one. This implies that the distance after encoding remains approximately preserved. Nevertheless, the distances are slightly distorted, which explains why the absolute similarity in Fig. 8 is lower for random ViTs than for the pixel values. In summary, shuffling reduces alignment even for the distance in terms of pixel values. This then transfers to random ViTs because these distances are approximately preserved.

D. On the *factorized* Hahn-Grant solver

In Sec. 4, we recap the Hahn-Grant solver [13] and introduce our *factorized* Hahn-Grant solver. Here, we provide more details on the implementation of the algorithms and show that both algorithms result in the same lower bounds. We also include an empirical study supporting the design choices behind our factorized Hahn-Grant solver: the factorization, faster LAP solvers, and finding primal solutions.

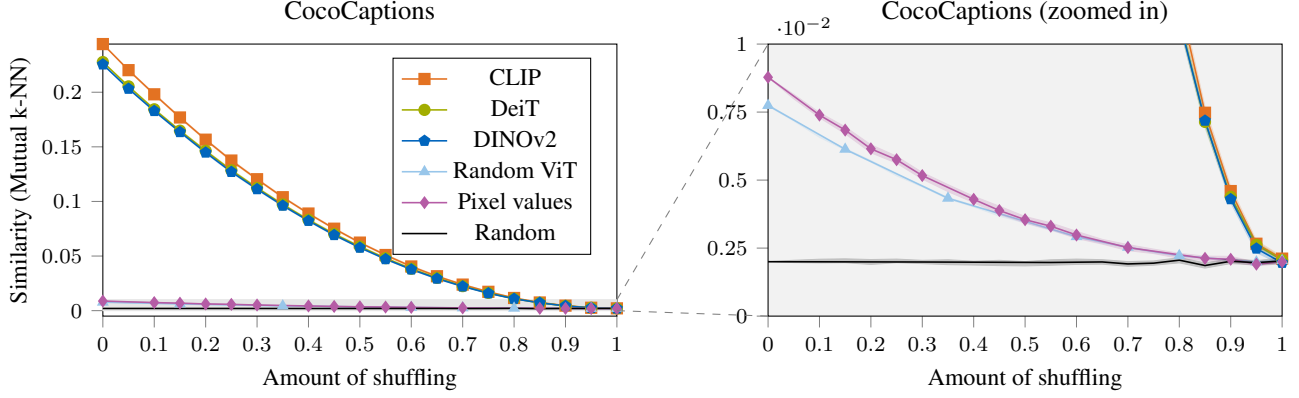


Figure 8. **Randomly initialized networks behave similarly to the pre-trained ones:** Zooming in (right) on the randomly initialized ViT, we observe a strikingly similar qualitative behavior – the similarity decreases monotonically with the increased degree of shuffling. This observation also holds for the curve resulting from raw pixel values. This surprising phenomenon presumably originates from the properties of the natural image manifold and the Lipschitz-continuity of neural networks.

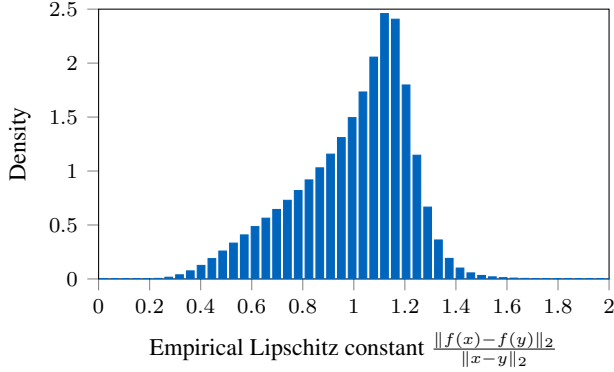


Figure 9. **Random networks roughly preserve distances:** Observe that the mode of the empirical Lipschitz constant is close to 1, which suggests that network encoding approximately preserves the distances in the input domain.

D.1. Proof of equivalence to Hahn-Grant solver

The main idea of the proof is that the lower bound, the *leader*, and all LAPs are the same for both algorithms. The main difference is that the dual vectors are stored in the tensors \mathbf{U} and \mathbf{V} instead of updating \mathbf{C} in-place.

First, we assume that $\mathbf{C}_{ijkl} = \mathbf{C}_{ik}^{(1)}\mathbf{C}_{jl}^{(2)}$ with $\mathbf{C}^{(1)}$ and $\mathbf{C}^{(2)}$ being non-negative and symmetric. Given this assumption, we will show that Algorithm 1 and Algorithm 2 are equivalent without our adaptations (Lines 4, 7, and 14) and using the Hungarian matching as the LAP solver. We will show that both algorithms have the same lower bound l , the *leader*, and the sum of complementary costs $\mathbf{C}_{ijkl} + \mathbf{C}_{klij}$. In particular, denoting the variables from Algorithm 2 with a bar, we have

$$l = \bar{l}, \quad \text{leader} = \overline{\text{leader}}, \quad \text{and} \quad (27)$$

$$\mathbf{C}_{ijkl} + \mathbf{C}_{klij} = 2\overline{\mathbf{C}}_{ik}^{(1)}\overline{\mathbf{C}}_{jl}^{(2)} - \overline{\mathbf{U}}_{ijk} - \overline{\mathbf{V}}_{ijl} - \overline{\mathbf{U}}_{kli} - \overline{\mathbf{V}}_{klj}.$$

for all $i \neq k, j \neq l \in [N]$. Starting with the first iteration until after Algorithm 1, Line 5 and Algorithm 2, Line 5, we have that the lower bound $l = \bar{l} = 0$ and

$$\text{leader} = \mathbf{C}_{ijij} = \mathbf{C}_{ii}^{(1)}\mathbf{C}_{jj}^{(2)} = \overline{\text{leader}} \quad (28)$$

are initialized the same. Furthermore, because $\overline{\mathbf{U}} = \overline{\mathbf{V}} = 0$, we have that

$$\mathbf{C}_{ijkl} = \mathbf{C}_{ik}^{(1)}\mathbf{C}_{jl}^{(2)} - \overline{\mathbf{U}}_{ijk} - \overline{\mathbf{V}}_{ijl}. \quad (29)$$

Thus, both algorithms have an equivalent starting condition.

Next, given that Eq. (27) holds, we show that both values are changed in an equivalent way. Given the same *leader* matrix, Line 6-8 from Algorithm 1 change l and *leader* in the same way as Lines 6-9 from Algorithm 2. Moreover, after Algorithm 1, Line 9 and Algorithm 2, Line 10, \mathbf{C}_{ijkl} and \mathbf{U}_{ijk} are changed in the same way. Therefore, the sum is also preserved:

$$\begin{aligned} & \mathbf{C}_{ijkl} + \mathbf{C}_{klij} \\ &= \mathbf{C}_{ijkl}^{\text{prev}} + \mathbf{C}_{klij}^{\text{prev}} + \frac{\text{leader}_{ij}}{N-1} + \frac{\text{leader}_{kl}}{N-1} \\ &= 2\overline{\mathbf{C}}_{ik}^{(1)}\overline{\mathbf{C}}_{jl}^{(2)} - \overline{\mathbf{U}}_{ijk}^{\text{prev}} + \frac{\text{leader}_{ij}}{N-1} - \overline{\mathbf{V}}_{ijl} \\ & \quad - \overline{\mathbf{U}}_{kli}^{\text{prev}} + \frac{\text{leader}_{kl}}{N-1} - \overline{\mathbf{V}}_{klj} \\ &= 2\overline{\mathbf{C}}_{ik}^{(1)}\overline{\mathbf{C}}_{jl}^{(2)} - \overline{\mathbf{U}}_{ijk} - \overline{\mathbf{V}}_{ijl} - \overline{\mathbf{U}}_{kli} - \overline{\mathbf{V}}_{klj}, \end{aligned} \quad (30)$$

where the superscript (prev) denotes the value before executing the line.

In Line 11 and Line 12 of Algorithm 1, the values from the complementary positions are redistributed to the current submatrix. Line 12 from Algorithm 2 also aggregates the sum of the complementary elements, albeit not by changing the cost matrices. Therefore, the sum of both elements remains the same. By definition of \mathbf{C}^{tmp} , it follows, that

Algorithm 1 Hahn-Grant solver [13]

```
1: Input:  $\mathbf{C} \in \mathbb{R}_{\geq 0}^{N \times N \times N \times N}$  cost tensor
2: Output:  $l \leq \arg \min_{\mathbf{P} \in \mathcal{P}_N} \sum_{i,j,k,l=1}^N \mathbf{C}_{ijkl} \mathbf{P}_{ij} \mathbf{P}_{kl}$ 
3:  $l \leftarrow 0$ 
4: while not converged do
5:    $\text{leader}_{ij} \leftarrow \mathbf{C}_{ijij}$  for  $i, j \in [N]$ 
6:    $\mathbf{u}, \mathbf{v}, - \leftarrow \text{hungarian\_matching}(\text{leader})$ 
7:    $l \leftarrow l + \sum_i \mathbf{u}_i + \sum_j \mathbf{v}_j$ 
8:    $\text{leader}_{ij} \leftarrow \text{leader}_{ij} - \mathbf{u}_i - \mathbf{v}_j$  for  $i, j \in [N]$ 
9:    $\mathbf{C}_{ijkl} \leftarrow \mathbf{C}_{ijkl} + \frac{\text{leader}_{ij}}{N-1}$  for  $i \neq k, j \neq l \in [N]$ 
10:  for  $i, j \in [N]$  do
11:     $\mathbf{C}_{ijkl} \leftarrow \mathbf{C}_{ijkl} + \mathbf{C}_{klij}$  for  $i \neq k, j \neq l \in [N]$ 
12:     $\mathbf{C}_{klij} \leftarrow 0$  for  $i \neq k, j \neq l \in [N]$ 
13:     $\mathbf{u}, \mathbf{v}, - \leftarrow \text{hungarian\_matching}(\mathbf{C}_{i,j,[N] \setminus \{i\}, [N] \setminus \{j\}})$ 
14:     $\mathbf{C}_{ijij} \leftarrow \sum_k \mathbf{u}_k + \sum_l \mathbf{v}_l$ 
15:     $\mathbf{C}_{ijkl} \leftarrow \mathbf{C}_{ijkl} - \mathbf{u}_k - \mathbf{v}_l$  for  $i \neq k, j \neq l \in [N]$ 
```

Algorithm 2 Factorized Hahn-Grant solver (Ours)

```
1: Input:  $\mathbf{C}^{(1)}, \mathbf{C}^{(2)} \in \mathbb{R}_{\geq 0}^{N \times N \times N \times N}$  symmetric cost tensors
2: Output:  $l \leq \arg \min_{\mathbf{P} \in \mathcal{P}_N} \sum_{i,j,k,l=1}^N \mathbf{C}_{ik}^{(1)} \mathbf{C}_{jl}^{(2)} \mathbf{P}_{ij} \mathbf{P}_{kl}$ ,
    $\mathbf{P}^* \in \mathcal{P}_N$  permutation matrix
3:  $l \leftarrow 0$ ;  $\mathbf{U}, \mathbf{V} \leftarrow \mathbf{0}_{N \times N \times N \times 1}$ ;  $\text{leader}_{ij} \leftarrow \mathbf{C}_{ii}^{(1)} \mathbf{C}_{jj}^{(2)}$ 
4:  $\mathbf{P}^* \leftarrow \text{primal\_heuristic}(\mathbf{C}^{(1)}, \mathbf{C}^{(2)})$ 
5: while not converged do
6:    $\mathbf{u}, \mathbf{v}, \mathbf{P} \leftarrow \text{lap\_solver}(\text{leader})$ 
7:    $\mathbf{P}^* \leftarrow \text{better}(\mathbf{P}^*, \mathbf{P})$ 
8:    $l \leftarrow l + \sum_i \mathbf{u}_i + \sum_j \mathbf{v}_j$ 
9:    $\text{leader}_{ij} \leftarrow \text{leader}_{ij} - \mathbf{u}_i - \mathbf{v}_j$  for  $i, j \in [N]$ 
10:   $\mathbf{U}_{ijk} \leftarrow \mathbf{U}_{ijk} - \frac{\text{leader}_{ij}}{N-1}$  for  $k \neq i, j \in [N]$ 
11:  for  $i, j \in [N]$  do
12:     $\mathbf{C}_{kl}^{\text{tmp}} \leftarrow 2\mathbf{C}_{ik}^{(1)} \mathbf{C}_{jl}^{(2)} - \mathbf{U}_{ijk} - \mathbf{V}_{ijl} - \mathbf{U}_{kli} - \mathbf{V}_{klj}$ 
   for  $i \neq k, j \neq l \in [N]$ 
13:     $\mathbf{u}, \mathbf{v}, \mathbf{P} \leftarrow \text{lap\_solver}(\mathbf{C}^{\text{tmp}})$ 
14:     $\mathbf{P}^* \leftarrow \text{better}(\mathbf{P}^*, \mathbf{P})$ 
15:     $\text{leader}_{ij} \leftarrow \sum_k \mathbf{u}_k + \sum_l \mathbf{v}_l$ 
16:     $\mathbf{U}_{ijk} \leftarrow \mathbf{U}_{ijk} + \mathbf{u}_k$  for  $i \neq k \in [N]$ 
17:     $\mathbf{V}_{ijl} \leftarrow \mathbf{V}_{ijl} + \mathbf{v}_l$  for  $j \neq l \in [N]$ 
```

Figure 10. **The Hahn-Grant solver (left) and the factorized Hahn-Grant solver (ours, right):** The Hahn-Grant solver [13] iteratively improves the dual bound of the QAP by solving linear assignment problems (LAPs). Our solver improves the memory requirements of the Hahn-Grant solver for factorized cost matrices, introduces a primal heuristic that reuses the assignment from the LAPs, and uses a faster solver for the LAPs.

$\mathbf{C}_{ijkl} = \mathbf{C}_{kl}^{\text{tmp}}$ and the Hungarian matching produces the same values for both algorithms. As the next step, the objective value is added to the leader in Algorithm 1 by first adding it to \mathbf{C}_{ijij} in Line 14 and then to leader_{ij} in Line 5 in the next iteration. In Algorithm 2, this value is directly added to leader_{ij} . Finally, the dual variables are subtracted from the cost in Line 15 of Algorithm 1 and Line 16 and Line 17 of Algorithm 2. This preserves the sum:

$$\begin{aligned} \mathbf{C}_{ijkl} + \mathbf{C}_{klij} &= \\ &= \mathbf{C}_{ijkl}^{\text{prev}} - \mathbf{u}_k - \mathbf{v}_l + \mathbf{C}_{klij}^{\text{prev}} - \mathbf{u}_i - \mathbf{v}_j \\ &= 2\overline{\mathbf{C}}_{ik}^{(1)} \overline{\mathbf{C}}_{jl}^{(2)} - \overline{\mathbf{U}}_{ijk}^{\text{prev}} - \mathbf{u}_k - \overline{\mathbf{V}}_{ijl}^{\text{prev}} - \mathbf{v}_l \\ &\quad - \overline{\mathbf{U}}_{kli}^{\text{prev}} - \mathbf{u}_i - \overline{\mathbf{V}}_{klj}^{\text{prev}} - \mathbf{v}_j \\ &= 2\overline{\mathbf{C}}_{ik}^{(1)} \overline{\mathbf{C}}_{jl}^{(2)} - \overline{\mathbf{U}}_{ijk} - \overline{\mathbf{V}}_{ijl} - \overline{\mathbf{U}}_{kli} - \overline{\mathbf{V}}_{klj}. \end{aligned} \quad (31)$$

Therefore, each iteration in both algorithms changes the costs in an equivalent way. As a result, the final bound l and each solution to the LAPs are the same. \square

In practice, we can also remove the non-negativity constraint because adding a constant to $\mathbf{C}^{(1)}$ or $\mathbf{C}^{(2)}$ leads to an equivalent optimization problem with an additional con-

stant term, *i.e.*

$$\begin{aligned} &\sum_{i,j,k,l=1}^N (\mathbf{C}_{ik}^{(1)} + c) \mathbf{C}_{jl}^{(2)} \mathbf{P}_{ij} \mathbf{P}_{kl} = \\ &= \sum_{i,j,k,l=1}^N \mathbf{C}_{ik}^{(1)} \mathbf{C}_{jl}^{(2)} \mathbf{P}_{ij} \mathbf{P}_{kl} + c \sum_{j,l=1}^N \mathbf{C}_{jl}^{(2)}. \end{aligned} \quad (32)$$

Therefore, we can subtract the minimal element from both matrices, apply the algorithm to the resulting non-negative matrices, and subtract the constant from Eq. (32) to the final objective value to retrieve the optimal objective value of the original problem.

D.2. Implementation details

We implement both Algorithm 2 and Algorithm 1 in Python using PyTorch [55]. The main computational bottleneck is the LAP solver. Therefore, we use a custom C++ algorithm for the forward-reverse auction [56] algorithm and for the Jonker-Volgenant algorithm [19, 31]. We stop the algorithm if the relative or absolute improvement of the dual bound l is smaller than $\varepsilon = 1e - 6$ or the primal objective is within ε of the dual bound. Finally, for the auction algorithm, a larger relaxation ε^{auc} usually leads to a faster runtime with the drawback of worse objectives and dual vectors. The Hahn-Grant algorithm also works for suboptimal dual vectors, but we observe that towards the end of the algorithm,

Solver	Cost	Bound
Hahn-Grant	-1.979877	-
+ factorized	-1.979875 \uparrow $2.0e^{-6}$	-2.089994 \uparrow
+ auction	-1.979871 \uparrow $4.3e^{-6}$	-1.981942 \uparrow $1.1e^{-1}$
+ Jonker-Volgenant	-1.979878 \downarrow $-7.3e^{-6}$	-1.980387 \uparrow $1.6e^{-3}$
+ LAP solutions	-1.979914 \downarrow $-3.5e^{-5}$	-1.980387 =
+ primal heuristic	-1.980015 \downarrow $-1.0e^{-4}$	-1.980387 =

Table 4. **Cost and bounds for our Hahn-Grant adaptation** ($N = 100$): The factorization and the auction algorithm slightly increase the cost of the solution, while leading to a small bound. The Jonker-Volgenant and especially the LAP solutions and primal heuristics also lead to better primal solutions.

better solutions in the LAPs are required. Therefore, we initialize $\epsilon^{\text{auc}} = 0.1$ relatively high in the beginning and multiply it with a factor of 0.9 in every iteration.

D.3. Ablations

Setup. We compare the original Hahn-Grant solver with our adaptation from Sec. 4: the factorization into matrices $\mathbf{C}^{(1)}$ and $\mathbf{C}^{(2)}$, using the auction algorithm or the Jonker-Volgenant as faster LAP solvers (Line 6 and Line 13), evaluating the individual LAP primal solutions (Line 7 and Line 14), and using primal heuristics (Line 4). For these experiments, we generate two sets with 100 vectors of dimensionality 1024 each, drawn element-wise from a standard normal distribution. These vectors are normalized, and the pairwise inner product is computed to produce two 100×100 similarity matrices. We apply all variations of the algorithms with a time limit of two hours to these cost matrices and evaluate the quality of the primal solutions and of the bound. We repeat the experiment with 5 random seeds and average the results. We also repeat the experiment with a set of 40 random vectors and a time limit of one hour.

Results. Tab. 4 shows the result for each adaptation for size 100 and Tab. 5 for size 40. We observe that the original Hahn-Grant solver reaches a non-trivial primal-dual bound for size 40 but does not finish the first iteration within the two hour time limit for size 100. Even though factorization was introduced for improved memory, it also slightly speeds up the computation, leading to a smaller bound for both sizes. The small increase in the objective for size 100 can be explained by the fact that the returned primal estimate is only the primal solution of the LAP for the `leader`. Therefore, the quality of this estimate can vary with every iteration. The auction and Jonker-Volgenant algorithms were introduced to improve the speed of the algorithm and, therefore, lead to smaller bounds. However, the Jonker-Volgenant algorithm leads to the tightest bounds empirically for large problems while the auction algorithm is slightly better on the size 40 problem. The LAP solutions do not change the dual estimate but improve the primal solution by

Solver	Cost	Bound
Hahn-Grant	-1.950160	-2.245823
+ factorized	-1.950166 \downarrow $-6.0e^{-6}$	-1.951418 \uparrow $2.9e^{-1}$
+ auction	-1.950197 \downarrow $-3.2e^{-5}$	-1.950586 \uparrow $8.3e^{-4}$
+ Jonker-Volgenant	-1.950197 \uparrow $3.9e^{-7}$	-1.950623 \downarrow $-3.8e^{-5}$
+ LAP solutions	-1.950268 \downarrow $-7.0e^{-5}$	-1.950623 =
+ primal heuristic	-1.950360 \downarrow $-9.2e^{-5}$	-1.950623 =

Table 5. **Cost and bounds for our Hahn-Grant adaptation** ($N = 40$): Our adaptations exhibit strong benefits either in terms of the solution cost or the tightness of the bound, frequently both. The auction algorithm leads to tighter bounds than the Jonker-Volgenant algorithm.

a significant margin. Finally, the primal heuristics further improve the primal solution. Since we are mostly interested in good primal solutions and measuring the quality of the solution, we use the algorithm with all the adaptations.

E. Experimental details

In this section, we provide more details supplementing the experiments in Sec. 5, which were excluded from the main text due to space constraints.

Our method only assumes pre-computed embeddings (or already pre-computed similarity matrices). Therefore, we are not limited to specific architectures or pre-training strategies. Our goal is to choose a variety of different architectures, pre-trainings, and model sizes for both modalities.

Vision models. We consider self-supervised, fully-supervised and vision-language supervised models with convolutional and vision transformer architectures of different capacities. For self-supervised methods, we consider different models from DINO [3] trained on ImageNet-1k [44] and models from DINOv2 [36] trained on LVD-142M. For supervised models, DeiT [48] and ConvNeXt [27] pre-trained on ImageNet-1k, ImageNet-22k [44] and a combination of both are used. Furthermore, we choose CLIP [42] as our vision-language model with both ResNet and ViT backbones. We use the code and models from the official repository except for ConvNeXt, where we use pre-trained models from the `timm` library. In total, we use 32 vision models.

Language models. Similar to the vision models, we consider different pre-trainings and network sizes. In particular, in addition to the CLIP [42] text models, contrastive learning, question-answer models, and average word embeddings are considered. We use the official CLIP repository for all CLIP text models and the SentenceTransformers [43] library for all other models. In total, we use 27 language models.

Datasets. We evaluate our experiments on CIFAR-10 [23], CINIC-10 [9], CIFAR-100 [23], and ImageNet-100 [44].

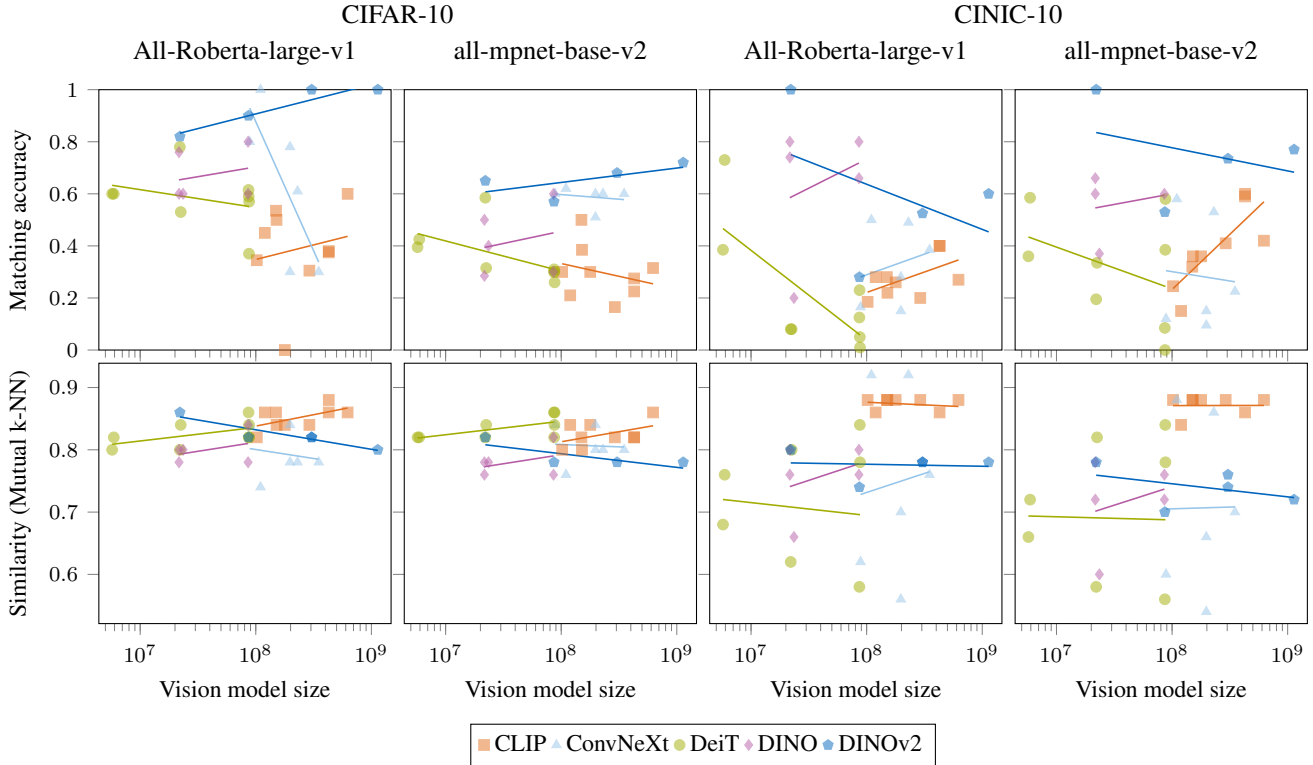


Figure 11. **Matching accuracy and Mutual k-NN on CIFAR-10 and CINIC-10:** Larger models do not necessarily lead to stronger alignment with language. Instead, it is the pre-training method that characterizes the vision-language alignment most. Here, DINOv2 yields the highest matching accuracy for both datasets and language models.

For ImageNet-100, we use the validation split and for all other datasets, we use the test split. We choose the same class names and prompts as ASIF [35] whenever available, and follow the same preprocessing as CLIP otherwise. For ImageNet-100, we observed an improved performance by encoding each class as “<name>: <definition>” using the WordNet definitions and more descriptive class names.

General setup. We implement all experiments in Python with PyTorch [55]. In general, we pre-compute the embeddings for each vision and language model and every dataset using PyTorch Lightning [57]. We do not use GPUs except for precomputing the embeddings. After computing the image-wise embeddings, we normalize them and average them for every class, see Eq. (1). The resulting object-wise embedding is again normalized. To evaluate the impact of small changes in the embeddings (and pairwise similarities), we only take a random subset of the image representations to compute the average. In particular, we use a half of the embeddings drawn uniformly for every random seed. For the language embeddings, we take the average over the embeddings for all different prompts.

Small-scale matching. We use 20 random seeds and all models on CIFAR-10 and CINIC-10 for small-scale match-

ing. In each experiment, we enumerate all permutations and compute all costs explicitly, returning the permutation with the minimal cost. The comparison of all combinations of vision and language models is given in Appx. F.1.

Larger-scale matching. For larger-scale matching, we use different subsets of classes using the optimization problem introduced in Sec. 4.2 solved with Gurobi [12]. For each problem size $N \in \{10, 20, \dots, 100\}$, we use the 10 best subset of classes, each with 3 random seeds for computing the object-level vision embeddings. We use our factorized Hahn-Grant solver and a time limit of one hour for each matching problem. The models are DINOv2 ViT-G/14, CLIP ViT-L/14@336px, and the distilled DeiT-B/16@384px with all-mpnet-base-v2.

Solver comparison. We evaluate the solvers both on small-scale and larger-scale matching. For small-scale matching, we use 20 random seeds for DINOv2 ViT-G/14, CLIP ViT-L/14@336px, and the distilled DeiT-B/16@384px with all-mpnet-base-v2 and All-Roberta-large-v1 on CIFAR-10 and CINIC-10. We present the results for all combinations in F.3. The larger-scale benchmark follows the setting of larger-scale matching, but only considers one out of the ten subsets and one random seed

Solver	Accuracy (%)	Matching Accuracy (%)
Random	12.1±10.3	12.5±11.6
LocalCKA	9.1±7.0	8.0±7.7
OT	5.4±9.5	4.5±9.4
FAQ	6.5±8.7	6.0±9.9
MPOpt	16.0±21.4	17.0±23.9
Ours	46.7±3.4	51.5±3.7
GT	85.2±0.6	100.0±0.0

Table 6. **Solver comparison on unsupervised classification:** Using DeiT and All-Roberta-large-v1, we show the accuracy of the unsupervised classifier for different solvers. The right column further shows how many of the centroids are mapped to the best class for the given cluster in line with the matching accuracy from the unsupervised matching experiments. Our QAP solver achieves a considerably higher matching and classification accuracy than the other methods.

for CIFAR-100 using CLIP ViT-L/14@336px and all-mpnet-base-v2 with a time limit of 1.5 hours.

Unsupervised classifier. For unsupervised classification, we use K-Means [28] to cluster image embeddings into prototype (object) embeddings. We use K-Means++ [58] from Scikit-learn [54] with 100 initializations. The cluster centers are then matched to the language embeddings using our factorized Hahn-Grant solver. Similar to the previous experiments, we only use a random 50% subset of the vision embeddings and evaluate the method for 20 random seeds. We report the results for DINOv2 ViT-G/14, CLIP ViT-L/14@336px, and the distilled DeiT-B/16@384px with all-mpnet-base-v2 and All-Roberta-large-v1 on CIFAR-10.

F. Evaluation results

Following up on Sec. 5, we report the results for all vision and language models in the small-scale matching setting (*cf.* Appx. F.1) and benchmark of the different solvers using multiple datasets and models (*cf.* Appx. F.2 and Appx. F.3).

F.1. Comparison of vision and language models

In this section, we report the results on the small-scale matching, spanning all vision and language models in our study. The results show, in particular, that DINOv2 outperforms the other models on both datasets and that the model size is less important than the pre-training method.

In Fig. 11, we show the matching accuracy (top) and Mutual k-NN with $k = 5$ (bottom) of each vision model in combination with All-Roberta-large-v1 (left) and all-mpnet-base-v2 (right) for CIFAR-10 (left) and CINIC-10 (right). The lines show the trend for increasing model sizes that are fitted to the models of varying capacity for each model class (different colors). The model size corresponds to the number of parameters. First, we observe that for both datasets and language models, DINOv2 yields the highest matching accuracy. Furthermore, for every model class,

there is no a clear propensity of larger models to perform better. As this seems to contradict the platonic representation hypothesis Huh et al. [17], we report the Mutual k-NN in the bottom plots. We observe that in line with our conclusions, there is still no clear improvement of the Mutual k-NN metric w.r.t. an increasing model capacity. This implies that larger models do not necessarily lead to stronger alignment with language – at least on CIFAR-10 and CINIC-10. Considering the observations by Huh et al. [17], this suggests that scaling the models could lead to a better alignment on the Wit dataset [59], even though it may not be sufficient to improve the alignment on every other dataset. We report the individual matching accuracy of each combination of vision and language model for CIFAR-10 in Fig. 12 and for CINIC-10 in Fig. 13.

F.2. Unsupervised classification: solver comparison

We also compare the solvers on the unsupervised classification setting in Tab. 6. In addition to the classification accuracy, we also report the matching accuracy. Given a clustering and the ground truth labels, we compute the optimal ground truth matching. The matching accuracy evaluates how well our unsupervised matching coincides with the ground truth matching. Finally, we report the performance when the ground truth matching is used instead of our unsupervised matching to evaluate the quality of the clustering.

Similar to the unsupervised matching experiments, we observe that our solver outperforms the other solvers in terms of both classification accuracy and matching accuracy. This means that our solver finds matches that agree well with the ground truth matches. We also observe that the k-means clustering is not perfect, and approximately 15% of the images are clustered in the wrong clusters. This hurts our clustering in two ways. First, since only whole clusters are assigned to classes, misclassified images will remain in the respective (wrong) cluster. Second, incorrect samples distort the centroids, which in turn can further affect the pairwise distances, leading to a worse matching. However, even with imperfect centroids, our matching finds non-trivial matches and leads to the first non-trivial unsupervised classification, which was not possible using previous local solvers.

F.3. Comparison of solvers on small-scale problems

Similar to Tab. 1, we benchmark different solvers for all combinations in Tab. 7. Our factorized Hahn-Grant solver and Gurobi [12] find the global optimum for all problems. For most combinations, these solvers are also the only solvers finding the global optimum. MPOpt [18] also finds the global optimum for some problems (*e.g.*, CIFAR-10 with DINOv2) but fails for other problems (*e.g.*, CIFAR-10 with CLIP). For all but two experiments (CIFAR-10 with DeiT and all-mpnet-base-v2 and CINIC-10 with DeiT and

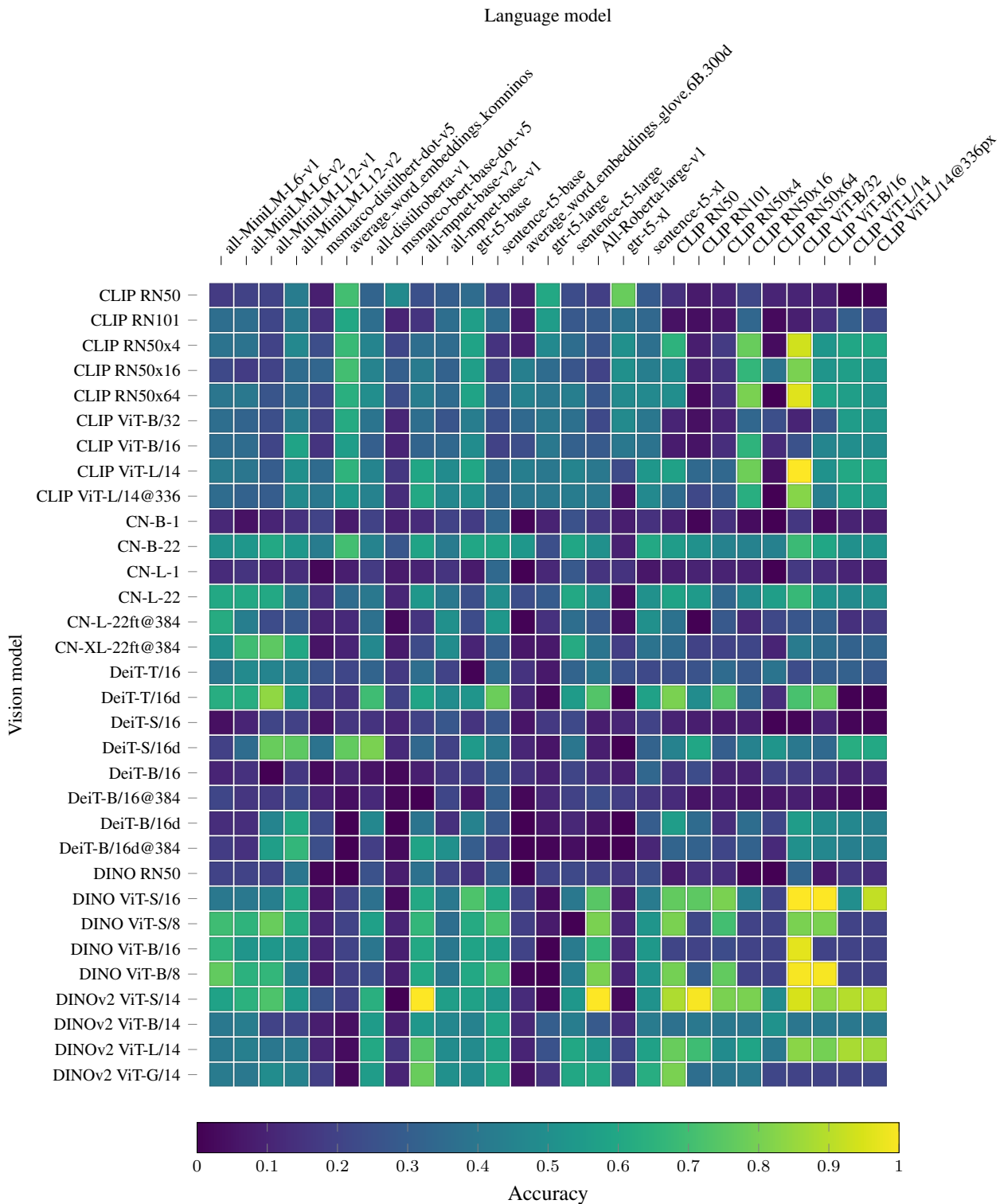


Figure 13. **Vision-language alignment accuracy on CINIC-10:** Here, DINO-based pre-training in conjunction with the CLIP-based text embedding exhibit a higher degree of conformity.

All-Roberta-large-v1), the global optimum also leads to the best matching accuracy, which underlines the importance of the Gromov-Wasserstein distance as a proxy measure for blind matching. Finally, the matching accuracy is close to random for most solvers (LocalCKA [30], OT [38], and FAQ [49]). This shows that a global solver is crucial to obtain non-trivial results.

G. Optimal transport as QAP solver

We show that optimal transport with uniform source and target probability distributions is equivalent to relaxing the QAP with doubly stochastic matrices. In our experiments, we use this equivalence to compare to the solutions from optimal transport solvers.

For uniform probability distributions $\mathbf{p} = \mathbf{q} = \frac{1}{N} \mathbb{1}$, let

$$\mathbf{T}^* \in \underset{\substack{\mathbf{T} \in [0,1]^{N \times N} \\ \mathbf{T} \mathbb{1} = \mathbf{p} \\ \mathbf{T}^T \mathbb{1} = \mathbf{q}}}{\arg \min} \mathbf{L}_{ijkl} \mathbf{T}_{ij} \mathbf{T}_{kl} \quad (33)$$

be an optimal transport matrix for the four axes tensor $\mathbf{L} \in \mathbb{R}^{N \times N \times N \times N}$. Then, for any other transport matrix $\mathbf{T} \in [0, 1]^{N \times N}$ with $\mathbf{T} \mathbb{1} = \mathbf{p}$ and $\mathbf{T}^T \mathbb{1} = \mathbf{q}$, it holds that

$$\mathbf{L}_{ijkl} \mathbf{T}_{ij} \mathbf{T}_{kl} \geq \mathbf{L}_{ijkl} \mathbf{T}^*_{ij} \mathbf{T}^*_{kl}. \quad (34)$$

Now, we can define our optimal stochastic matrix $\mathbf{S}^* \in [0, 1]^{N \times N}$ by $\mathbf{S}^* = N \mathbf{T}^*$. This is indeed a stochastic matrix as $N \mathbf{T}^* \geq 0$, $\mathbf{S}^* \mathbb{1} = N \mathbf{T}^* \mathbb{1} = N \mathbf{p} = \mathbb{1}$ and $(\mathbf{S}^*)^T \mathbb{1} = N \mathbf{T}^{*T} \mathbb{1} = N \mathbf{q} = \mathbb{1}$. Moreover, this stochastic matrix is optimal, because for every other stochastic matrix $\mathbf{S} \in [0, 1]^{N \times N}$,

$$\begin{aligned} \mathbf{L}_{ijkl} \mathbf{S}_{ij} \mathbf{S}_{kl} &= N^2 \mathbf{L}_{ijkl} \frac{\mathbf{S}_{ij}}{N} \frac{\mathbf{S}_{kl}}{N} \geq \\ &\geq N^2 \mathbf{L}_{ijkl} \mathbf{T}^*_{ij} \mathbf{T}^*_{kl} = \mathbf{L}_{ijkl} \mathbf{S}^*_{ij} \mathbf{S}^*_{kl}. \end{aligned} \quad (35)$$

Here, we use the fact that $\frac{\mathbf{S}}{N}$ is a valid transport matrix as $\frac{\mathbf{S}}{N} \mathbb{1} = \frac{1}{N} \mathbb{1} = \mathbf{p}$ and $\frac{\mathbf{S}^T}{N} \mathbb{1} = \frac{1}{N} \mathbb{1} = \mathbf{q}$. The other direction can be derived in a similar way by dividing the doubly stochastic matrix by N .

References

- [54] Fabian Pedregosa, Gaël Varoquaux, and Alexandre Gramfort, et al. Scikit-learn: Machine learning in Python. In *JMLR*, 2011. [viii](#)
- [55] Adam Paszke, Sam Gross, and Francisco Massa, et al. PyTorch: An imperative style, high-performance deep learning library. In *NeurIPS*, 2019. [v, vii](#)
- [56] Dimitri P. Bertsekas and David A. Castanon. In *Comput. Optim. Appl. 1*, pages 277-297, 1992. [v](#)
- [57] William Falcon et al. PyTorch Lightning. <https://github.com/Lightning-AI/lightning>, 2019. [vii](#)
- [58] Arthur David and Sergei Vassilvitskii. k-means++: The advantages of careful seeding. In *Proc. 18th Annu. ACM-SIAM Sympos. Discrete Algorithms*, pages 1027–1035, 2007. [viii](#)
- [59] Krishna Srinivasan, Karthik Raman, Jiecao Chen, et al. Wit: Wikipedia-based image text dataset for multimodal multilingual machine learning. In *SIGIR*, pages 2443-2449. 2021. [viii](#)

		All-Roberta-large-v1			all-mpnet-base-v2				
		Accuracy (%)	Cost	Global? (%)	Accuracy (%)	Cost	Global? (%)		
CIFAR-10	CLIP	Random	8.5±10.4	1.77±0.32	0.0±0.0	8.5±10.4	1.8 ±0.29	0.0±0.0	
		LocalCKA [30]	9.5±8.87	1.82±0.33	0.0±0.0	12.5±11.64	1.72±0.31	0.0±0.0	
		OT [38]	11.0±3.08	0.67±0.03	0.0±0.0	0.0±0.0	0.36±0.01	0.0±0.0	
		FAQ [49]	1.5±3.66	0.78±0.06	0.0±0.0	5.0±8.89	0.36±0.02	20.0±41.04	
		MPOpt [18]	0.0±0.0	0.51±0.01	0.0±0.0	0.0±0.0	0.6 ±0.01	0.0±0.0	
		Gurobi [12]	38.0±10.05	0.4 ±0.01	100.0±0.0	22.5±4.44	0.33±0.01	100.0±0.0	
		Ours	38.0±10.05	0.4 ±0.01	100.0±0.0	22.5±4.44	0.33±0.01	100.0±0.0	
	DeiT	Random	8.5±10.4	1.77±0.29	0.0±0.0	8.5±10.4	1.81±0.27	0.0±0.0	
		LocalCKA [30]	10.0±9.18	1.85±0.2	0.0±0.0	6.0±6.81	1.77±0.22	0.0±0.0	
		OT [38]	0.0±0.0	0.84±0.01	0.0±0.0	19.0±3.08	0.28±0.01	30.0±47.02	
		FAQ [49]	22.5±10.7	0.36±0.13	0.0±0.0	37.0±14.9	0.3 ±0.01	0.0±0.0	
		MPOpt [18]	0.0±0.0	0.74±0.02	0.0±0.0	0.0±0.0	0.72±0.01	0.0±0.0	
		Gurobi [12]	57.0±4.7	0.27±0.01	100.0±0.0	26.0±6.81	0.27±0.0	100.0±0.0	
		Ours	57.0±4.7	0.27±0.01	100.0±0.0	26.0±6.81	0.27±0.0	100.0±0.0	
	DINOv2	Random	8.5±10.4	1.8 ±0.27	0.0±0.0	8.5±10.4	1.82±0.28	0.0±0.0	
		LocalCKA [30]	14.0±11.42	1.75±0.31	0.0±0.0	7.5±9.1	1.67±0.24	0.0±0.0	
		OT [38]	24.5±26.25	0.63±0.44	0.0±0.0	24.0±24.15	1.13±0.54	5.0±22.36	
		FAQ [49]	34.0±35.3	0.49±0.18	5.0±22.36	39.0±23.82	0.65±0.22	0.0±0.0	
		MPOpt [18]	100.0±0.0	0.33±0.01	100.0±0.0	72.0±17.65	0.45±0.01	100.0±0.0	
		Gurobi [12]	100.0±0.0	0.33±0.01	100.0±0.0	72.0±17.65	0.45±0.01	100.0±0.0	
		Ours	100.0±0.0	0.33±0.01	100.0±0.0	72.0±17.65	0.45±0.01	100.0±0.0	
	CINIC-10	CLIP	Random	8.5±10.4	1.76±0.31	0.0±0.0	8.5±10.4	1.73±0.3	0.0±0.0
			LocalCKA [30]	14.5±8.87	1.81±0.25	0.0±0.0	10.0±8.58	1.77±0.27	0.0±0.0
			OT [38]	1.5±3.66	1.06±0.13	0.0±0.0	1.5±3.66	0.64±0.11	0.0±0.0
FAQ [49]			27.5±5.5	0.37±0.02	0.0±0.0	1.0±3.08	0.62±0.08	0.0±0.0	
MPOpt [18]			39.5±2.24	0.36±0.04	95.0±22.36	49.0±12.1	0.36±0.02	50.0±51.3	
Gurobi [12]			40.0±0.0	0.35±0.01	100.0±0.0	60.0±0.0	0.34±0.02	100.0±0.0	
Ours			40.0±0.0	0.35±0.01	100.0±0.0	60.0±0.0	0.34±0.02	100.0±0.0	
DeiT		Random	8.5±10.4	1.73±0.25	0.0±0.0	8.5±10.4	1.74±0.25	0.0±0.0	
		LocalCKA [30]	9.0±7.88	1.9 ±0.17	0.0±0.0	6.5±8.75	1.66±0.22	0.0±0.0	
		OT [38]	37.0±6.57	0.38±0.02	0.0±0.0	3.0±4.7	0.51±0.05	0.0±0.0	
		FAQ [49]	29.5±17.01	0.38±0.07	0.0±0.0	9.0±3.08	0.58±0.04	0.0±0.0	
		MPOpt [18]	3.5±4.89	0.31±0.01	55.0±51.04	58.0±6.16	0.49±0.01	100.0±0.0	
		Gurobi [12]	1.0±3.08	0.31±0.01	100.0±0.0	58.0±6.16	0.49±0.01	100.0±0.0	
		Ours	1.0±3.08	0.31±0.01	100.0±0.0	58.0±6.16	0.49±0.01	100.0±0.0	
DINOv2		Random	8.5±10.4	1.79±0.23	0.0±0.0	8.5±10.4	1.76±0.23	0.0±0.0	
		LocalCKA [30]	10.5±9.45	1.96±0.14	0.0±0.0	13.0±7.33	1.68±0.21	0.0±0.0	
		OT [38]	50.5±15.72	0.65±0.06	35.0±48.94	14.0±5.03	0.96±0.22	0.0±0.0	
		FAQ [49]	52.5±13.33	0.65±0.06	0.0±0.0	9.0±10.21	0.91±0.12	0.0±0.0	
		MPOpt [18]	60.0±0.0	0.6 ±0.02	95.0±22.36	73.0±13.8	0.66±0.03	90.0±30.78	
		Gurobi [12]	60.0±0.0	0.6 ±0.02	100.0±0.0	77.0±7.33	0.65±0.02	100.0±0.0	
		Ours	60.0±0.0	0.6 ±0.02	100.0±0.0	77.0±7.33	0.65±0.02	100.0±0.0	

Table 7. **Vision-language alignment on CIFAR-10 and CINIC-10.** Our QAP solver achieves predominantly favourable matching accuracy, cost and optimality guarantees – even in comparison to proprietary solvers (Gurobi). This holds across two datasets and three pre-trained models: CLIP, DeiT and DINOv2.